SANDIA REPORT

SAND2014-17957
Unlimited Release
Printed September 2014

Self-deconstructing algae biomass as feedstock for transportation fuels

Ryan W. Davis

Prepared by
Sandia National Laboratories
Albuquerque, New Mexico 87185 and Livermore, California 94550

Sandia National Laboratories is a multi-program laboratory managed and operated by Sandia Corporation, a wholly owned subsidiary of Lockheed Martin Corporation, for the U.S. Department of Energy's National Nuclear Security Administration under contract DE-AC04-94AL85000.

Approved for public release; further dissemination unlimited.

Issued by Sandia National Laboratories, operated for the United States Department of Energy by Sandia Corporation.

NOTICE: This report was prepared as an account of work sponsored by an agency of the United States Government. Neither the United States Government, nor any agency thereof, nor any of their employees, nor any of their contractors, subcontractors, or their employees, make any warranty, express or implied, or assume any legal liability or responsibility for the accuracy, completeness, or usefulness of any information, apparatus, product, or process disclosed, or represent that its use would not infringe privately owned rights. Reference herein to any specific commercial product, process, or service by trade name, trademark, manufacturer, or otherwise, does not necessarily constitute or imply its endorsement, recommendation, or favoring by the United States Government, any agency thereof, or any of their contractors or subcontractors. The views and opinions expressed herein do not necessarily state or reflect those of the United States Government, any agency thereof, or any of their contractors.

Printed in the United States of America. This report has been reproduced directly from the best available copy.

Available to DOE and DOE contractors from
U.S. Department of Energy
Office of Scientific and Technical Information
P.O. Box 62
Oak Ridge, TN 37831

Telephone: (865) 576-8401
Facsimile: (865) 576-5728
E-Mail: reports@adonis.osti.gov
Online ordering: http://www.osti.gov/bridge

Available to the public from
U.S. Department of Commerce
National Technical Information Service
5285 Port Royal Rd.
Springfield, VA 22161

Telephone: (800) 553-6847
Facsimile: (703) 605-6900
E-Mail: orders@ntis.fedworld.gov
Online order: http://www.ntis.gov/help/ordermethods.asp?loc=7-4-0#online

SAND2014-17957
Unlimited Release
Printed September 2014

Self-deconstructing algae biomass as feedstock for transportation fuels

Ryan W. Davis
08634 Biomass Science and Conversion Technologies
Sandia National Laboratories
P.O. Box 969
Livermore, California 94550-MS9671

Abstract

The potential for producing biofuels from algae has generated much excitement based on projections of large oil yields with relatively little land use. However, numerous technical challenges remain for achieving market parity with conventional non-renewable liquid fuel sources. Among these challenges, the energy intensive requirements of traditional cell rupture, lipid extraction, and residuals fractioning of microalgae biomass have posed significant challenges to the nascent field of algal biotechnology. Our novel approach to address these problems was to employ low cost solution-state methods and biochemical engineering to eliminate the need for extensive hardware and energy intensive methods for cell rupture, carbohydrate and protein solubilization and hydrolysis, and fuel product recovery using consolidated bioprocessing strategies. The outcome of the biochemical deconstruction and conversion process consists of an emulsion of algal lipids and mixed alcohol products from carbohydrate and protein fermentation for co-extraction or *in situ* transesterification.

ACKNOWLEDGMENTS

The author would like to acknowledge Ben C. Wu for instructive discussions regarding the challenges facing cost-effective production of biofuels from algae.

CONTENTS

FIGURES

TABLES

1. INTRODUCTION

Biofuels from algae present the possibility of eliminating the cycle of food versus fuel crises for energy feedstock production. However, reduction of production costs and energy requirements is paramount for establishing an economical algae biofuels industry. Furthermore, the basic chemical profile of microalgae - roughly equal ratios of lipids, proteins, and polysaccharides - requires that the value of the biomass be optimized by making use of all of the algal biochemical components (Wijffels et al., 2010). To date, a limited number of microalgal strains have been successfully cultured at commodity scales in saline media. Following production of the algal biomass, an additional hurdle lies in converting the cellular material into a form suitable for fuels production (Greenwell et al., 2010; Molina Grima et al., 2003). This conversion requires rupturing the algal cell walls for releasing the lipids, and breaking down the protein and polysaccharide fractions to generate a viable medium for fermentative conversion. Current technologies being pursued to perform these functions include mechanical disruption, solvent extraction, sonication, pulsed electric fields, pyrolysis, supercritical fluids, microwave irradiation, and enzymatic processing (Mercer & Armenta, 2011). However, each of these approaches requires significant energetic and hardware requirements. In this effort we sought to combine cell rupture, lipid extraction, and residuals processing in a low-cost biologically engineered process based on expression of deconstruction genes for solubilization and hydrolysis of the protein and polysaccharide structural fractions of industrially relevant microalga. Previous successes for employing a similar strategy for terrestrial feedstocks suggest that this functionality is feasible (Taylor et al., 2008), although the methods for implementing this capability in microalgae are not well established.

Until recently, little progress has been made employing biological engineering for microalgal biofuels applications. However, recent achievements in genetic analysis and minimally perturbative methods of algal transformation have opened the gates for new research in this area. A prime target for employing biological engineering is the development of biochemically triggered expression of 'deconstruction genes' for depolymerizing algal proteins, the cell wall, and extracellular matrix (ECM) analogue. Not only would such process lead to a low cost lipid extraction process, but the polysaccharides and proteins that compose the ECM and residual biomass could be simply solubilized and hydrolyzed to sugars and amino acids for subsequent fermentation. In this work, we describe results of low intensity chemical and biochemical deconstruction and conversion of algae. Finally, we coupled expression of exogenous mesophilic cellulase and protease enzymes to genes involved in responding to nutrient limitation and subsequent lipid accumulation for programmed autolysis. The results indicate progress towards means for achieving maximal net biomass productivity, biological deconstruction, and conversion of all of the major biochemical fractions to liquid fuels.

In addition to the basic biotechnological challenge of establishing metabolically triggered expression of exogenous proteo- and cellulolytic enzymes in industrially relevant microalga, several additional factors must be addressed to suit the specific physiological details of algae. Foremost among these factors is the fact that a detailed understanding of cell wall and ECM

structure - the basis of recalcitrance - is lacking for microalgae. Fortunately, unlike conventional woody biomass, algae lack the lignin biochemical component that underlies the extreme hydrolytic stability observed in this feedstock. However, algal cell walls have their own set of challenges, including an elevated overall glycoprotein fraction, as well as the presence of polysaccharide crosslinking linear polyethers, known as algaenans (Gelin et al., 1997). With a better understanding of microalgal cell wall/ECM chemical composition and structure, we can begin to combat downstream processing challenges including selection of the potential enzyme expression cocktails for achieving efficient cell wall deconstruction, lipid liberation, and conversion of the residuals in a saline environment.

A novel and low cost alternative to production and purification of proteo- and cellulolytic enzymes from conventional fungal sources is to use biological engineering to port this function directly to an algal species relevant for biofuels production. However, several biological criteria must be met for generating a sustainable, self-deconstructing microalgal biomass source. These criteria include, 1) culture stability in a wide range of outdoor environments, 2) substantial biomass productivity, 3) tolerance to saline and otherwise compromised liquid media sources, and 4) the availability of effective mechanisms of genetic transformation. Currently, only two species meet these criteria: *Dunaliella salina* and *Nannochloropsis* sp.

Dunaliella salina, a halophilic chlorophyte common to marine waters, is among the most commercially relevant algal strains worldwide. *Dunaliella* has been produced at industrial scale in outdoor cultivation facilities for a variety of value-added and antioxidant compounds used in the neutraceutical, cosmetic, and biochemical industries (Borowitzka, 1986). Additionally, *D. salina* has lipid and fatty acid compositions that are suitable feedstocks for biofuel production by transesterification (Tornabene et al., 1980). Finally, recent reports of successful nuclear transformation of *Dunaliella salina* (Tan et al., 2005) provide the basic groundwork for employing methods of biological engineering in this species. *Nannochloropsis* sp. is a similarly halotolerant microalgal strain that has shown considerable promise for large scale production in outdoor settings. Based on a two-phase growth scheme, this strain has been reported to generate large quantities of lipids, projected to total oil yields greater than 90 kg per hectare per day (Rodolfi et al., 2009). Additionally, *Nannochloropsis* sp. has the capability to produce valuable co-products, especially hydroxylated carotenoids, including astaxanthin and zeaxanthin. Finally, a recent report of homologous recombination (HR) in *Nannochloropsis sp.* presents the distinct possibility for high efficiency genetic transformation of this species (Kilian et al., 2011).

Based on the rationale described above, we pursued a path to understand and develop the means for implementation of a "self-deconstructing" algae biomass strategy for triggering cell rupture, lipid extraction, and residuals processing with minimal energetic and infrastructural requirements. In the first phase of the research, we used Sandia National Laboratories' unique chemical imaging and spectroscopic capabilities to characterize energy metabolite production in *Dunaliella salina* and *Nannochloropsis* sp in vivo. By then coupling the imaging capability with established methods for detecting proteo- and cellulolytic activity (DNS and BCA colorimetry), we evaluated a variety of combinations of chemical, osmotic, and enzymatic treatments to obtain optimal cellular deconstruction, and subsequent solubilization and hydrolysis of the carbohydrate and protein fractions of the biomass. General classifications of enzymes to be assayed include endoglucanases, cellobiohydrolases, β-glucanases, endoxyalanases, pectinases, and endopeptidases. Of particular interest for this application were halophilic enzymes originating from the prolifically cellulolytic fungi, *Aspergillus niger* and *Trichoderma reesei*; and natural predators of marine microalgae, especially *Aplodactylus punctatus* and *Helix pomatia*. In

addition to the proteomic details of the enzymes themselves, the impact of the state variables osmolarity and temperature were also considered.

Parallel to the combinatorial assessment of proteo- and cellulolytic enzymes, we undertook undertake a focused effort to establish successful transformation of the more recalicatrant strain, *Nannochloropsis* sp., using electroporation. Specifically, we sought to facilitate HR transformation of *Nannochloropsis* using the *VCP2* bidirectional promoter and a *Sh ble* selection marker, which has been previously reported to enable unselected cotransformation as well as coupling of genes to the promoter in the opposite direction of the selection marker. The recent elucidation of the organelle genomes of *Nannochloropsis* (Wei et al., 2013) facilitates the potential for developing a chloroplast transformation protocol for this species, which is the preferred method for producing high quantities of recombinant proteins, including deconstruction enzymes. For this effort, we employed the highly expressed rbcl and psbB sequences and their corresponding promoter and terminator regions, in conjunction with a mutated psba gene which confers resistance to the common herbicide, 3-(3,4-dichloropheyl)-1,1-dimethylurea (DCMU). Electroporation-based transformation will be optimized by imaging the impact of applied voltage, capacitance, and shunt resistance on the *Dunaliella* ECM and cellular ultrastructure, as well as by varying the quantity and type (linear or circular) of DNA used. Nuclear transformation was also attempted using the halotolerant phleomycin-binding protein from *Streptoallotecichus hindustanus*. For this effort, expression was driven using the highly expressed Rbcs genes and their associated 5' and 3' regulatory regions. A particular challenge that was introduced at this phase of the research was preventing the activity of the expressed deconstruction enzymes to allow maximum biomass accumulation prior to deconstruction. Fortunately, temperature is a primary regulator of most cellulolytic enzymes. For our initial investigations, we used mesophilic enzymes with minimal activity under conditions supporting algal growth (~15 - 30°C), with triggering in a subsequent heating cycle tailored for deconstruction. At this stage, several important questions were addressed concerning transgenetically expressed deconstruction enzymes in alga, including 1) the effect on total biomass and biomolecule production, 2) the relative functionality of the resulting enzymes, and 3) the competing roles of intracellular trafficking, compartmentalization, and excretion of the enzymes. Subsequently, two mechanisms were pursued to maximize deconstruction efficacy. First, we attempted to couple the respective genes to promoters responding to nutrient limitation (e.g. acetyl-CoA carboxylase, ACC), to accelerate enzyme expression immediately prior to deconstruction. Second, we investigated methods for encoding the enzymes into cellulosome complexes for increased cellulolytic functionality.

2.1. Label-free imaging of algae biomass

Current methods for identifying algae strains and growth conditions that support high biomass and lipid production require a variety of fluorescent chemical indicators, such as Nile Red and more recently, Bodipy. Despite notable successes using these approaches, chemical indicators exhibit several drawbacks, including non-uniform staining, low lipid specificity, cellular toxicity, and variable permeability based on cell-type, limiting their applicability for high-throughput bioprospecting. In this work, we used *in vivo* hyperspectral confocal fluorescence microscopy of a variety of potential microalgae production strains (*Nannochloropsis sp.*, *Dunaliella salina*, *Neochloris oleoabundans*, and *Chlamydomonas rheinhardtii)* to identify a label-free method for

localizing lipid bodies and quantifying the lipid yield on a single-cell basis. By analyzing endogenous fluorescence from chlorophyll and resonance Raman emission from lipid-solubilized carotenoids we deconvolved pure component emission spectra and generated diffraction limited projections of the lipid bodies and chloroplast organelles, respectively. Applying this imaging method to nutrient depletion time-courses from lab-scale and outdoor cultivation systems revealed an additional autofluorescence spectral component that became more prominent over time, and varied inversely with the chlorophyll intensity, indicative of physiological compromise of the algal cell. This signal could result in false-positives for conventional measurements of lipid accumulation (via spectral overlap with Nile Red), however, the additional spectral feature was found to be useful for classification of lipid enrichment and culture crash conditions in the outdoor cultivation system. Under nutrient deprivation, increases in the lipid fraction of the cellular volume of ~500% were observed, as well as a correlated decrease in the chloroplast fraction of the total cellular volume. The results suggest that a membrane recycling mechanism dominates for nutrient deprivation-based lipid accumulation in the microalgae tested. These results were published in Davis et al *Algal Research* 2014 and support identification of lipid enrichment and culture degradation in a number of algal production strains (Davis et al., 2013). Important findings are described briefly below.

2.2. Devlopement of a label-free imaging technique for algal lipids

In order to develop a fluorescence imaging technique that does not rely on exogenous fluorophores to label the cellular components of interest, one must be able to detect endogenous fluorescent components that can be used as an internal label. A surrogate endogenous fluorophore was desired that could report of the total amount of lipid that is produced in the algae. Carotenoids have been reported to be localized and stored within algal lipid droplets (Kleinegris et al., 2010; Lemoine & Schoefs, 2010; Moulin et al., 2010), therefore carotenoids can be used for this application. Kleinegris et al. have shown the use of carotenoid fluorescence to visualize lipid in algal cells using a filter-based microscope (Kleinegris et al., 2010). However, although carotenoid co-exists in the lipid droplets, carotenoid is also present within the thylakoid membranes of the chloroplast itself. Therefore, to be able quantify the amount of lipid present within an algal cell, the carotenoid signal that is in lipids must be differentiated from that from that in the thylakoid membranes of the chloroplast. Using a filter based microscope to isolate and quantify the amount of lipid within algal cells is problematic due to cross talk between these signal sources.

Two different laser powers were explored for our approach (figure 1). Low power laser excitation (50 W/cm^2 at the sample) primarily provided spectral information relating to Chlorophyll-*a* (Chl-*a*) contained within the chloroplast. This power was used to prevent saturation of the EMCCD detector and excessive noise contributions from the highly emissive Chl-*a* spectral component. Figure 1A shows an example of the mean spectrum and mean image from a single cell using this power level. In order to obtain spectral information on the carotenoid pool, we increased the laser power by a factor of 300x (figure 1b). However, this required addition of an absorptive filter to attenuate the excessive fluorescence from Chl-*a*, with minimal loss of carotenoid emission (see materials and methods). The Figure 1C shows the transmission profile of the absorptive emission filter that was employed. This filter preferentially weights our spectral data to increase our detection and sensitivity for carotenoid, however still retain the valuable information about the chloroplast as characterized by the Chl-*a*

signal. Notice that the image from the lower laser power (figure 1a) shows just the chloroplast, whereas the same confocal optical section of the same cell in figure 2b shows the same chloroplast along with a new feature that is attributed to a lipid globule. To illustrate that the carotenoid signature due to the chloroplast is highly overlapped with the carotenoid present in the lipid, the mean spectra taken for the colored regions of interest in the image are shown in figure 2b. The green colored region is the chloroplast and is represented by the green trace, whereas the red colored region is from the lipid globule and is represented by the red trace. The spectrum from the chloroplast shows an attenuated Chl-*a* signature along with carotenoid fluorescence, whereas the lipid region primarily shows the carotenoid fluorescence.

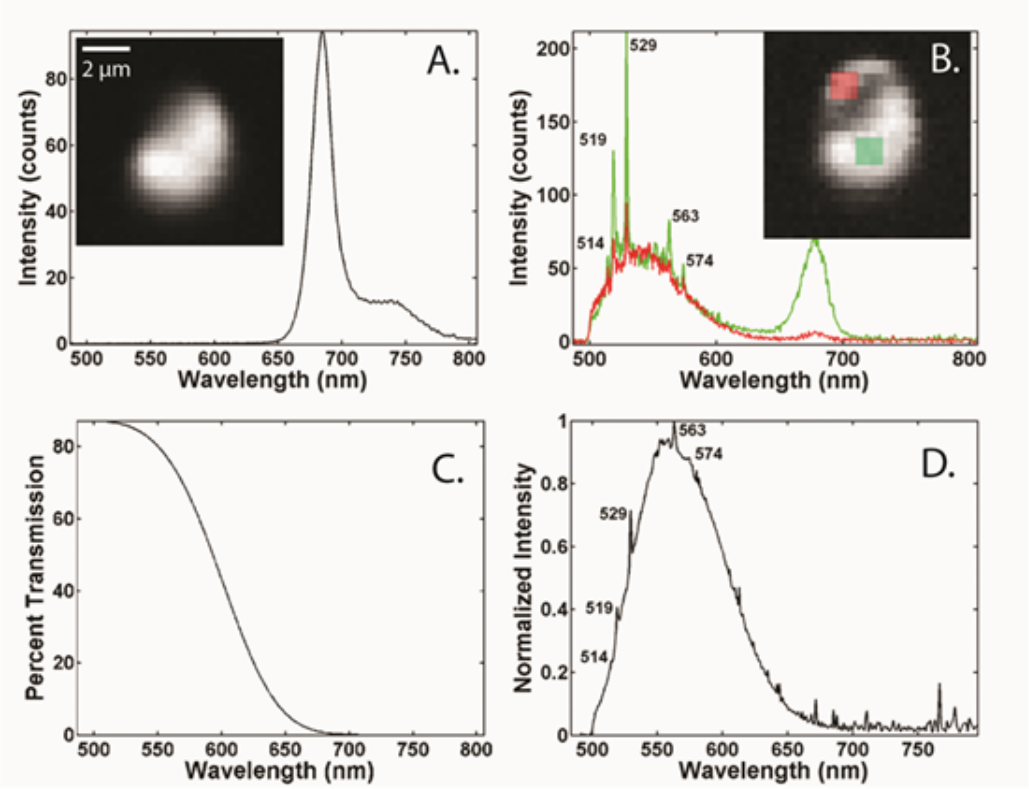

Figure 1. (A.) Mean spectrum and associated mean image of a single *Nannochloropsis sp.* cell using low laser excitation power. (B.) Mean spectrum and associated mean image of the same algal cell as seen in 1a at a higher laser power. The major resonance enhanced Raman bands related to carotenoid are labeled next to the peaks. (C.) Transmission curve of the absorption filter used to enhance the carotenoid signal and down weight the chlorophyll intensity. (D.) Fluorescence of beta-carotene dissolved in low fluorescing immersion oil. Resonance enhanced bands are labeled to confirm that the peaks in 1b are associated with beta-carotene.

The sharp peaks within these spectra are not due to noise; instead they are a result of resonance enhanced Raman bands. Typically, Raman bands would not be observed in a fluorescence measurement; however, resonance enhancement arising from absorption of the excitation laser near the electronic transition of the carotenoids is sufficient to amplify a subset of Raman-active modes by several orders of magnitude (Robert, 1999a). Figure 1D is a spectrum of β-carotene dissolved in low fluorescence immersion oil (Zeiss Immersol 518F) and collected under the same instrumental conditions as the algae cell shown in the figure. Although

the fluorescence appears to be slightly shifted compared with the carotenoid fluorescence from the algal cell, the Raman bands correspond directly with that of the algal cell, confirming the spectral assignment as carotenoid resonance Raman features. Specifically, these bands correspond to three major vibrational modes of carotenoids, the C=C stretch (1529±10 cm^{-1} or 527 nm), the C-C stretch (1157±10 cm^{-1} or 519 nm), and a C-C bend (1004±10 cm^{-1} or 514 nm). Although progressive shifts in the wavenumber of the C=C stretching band are correlated to increased polyene chain length, deviations in the exact frequency shift should be expected by interactions with the host matrix (de Oliveira et al., 2010).

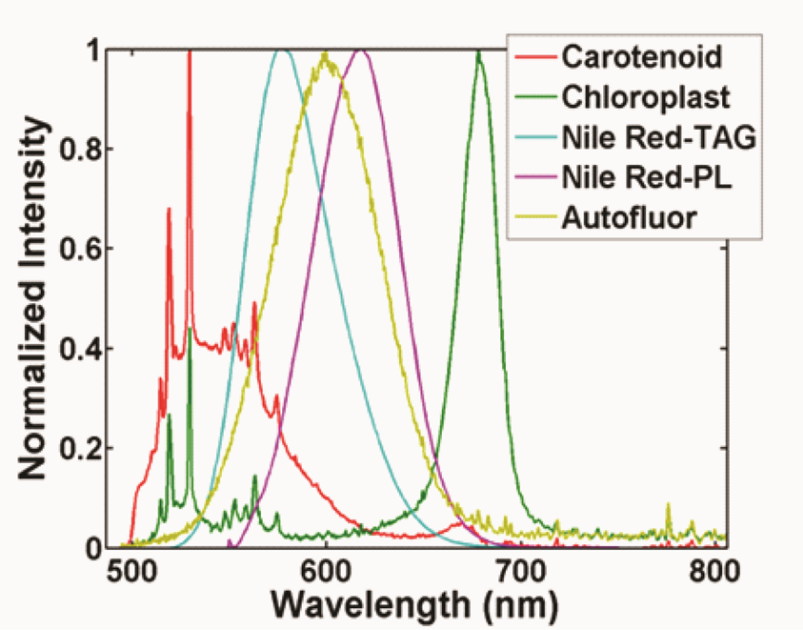

Figure 2. MCR pure spectral components extracted from the hyperspectral images of *Nannochloropsis sp*. The carotenoid component (green) is present in both the lipid and the thylakoids of the chloroplast. The chloroplast component consists of both Chl-*a* and resonance enhanced Raman bands associated with carotenoid. There were two components for Nile Red. Nile Red stains neutral lipid or triacylglycerol (TAG) which is blue-shifted of the Nile Red bound to phospholipid (PL). The autofluorescence emission (Autofluor) is a component that is associated with senescent cultures.

Following this confirmation that hyperspectral confocal microscopy has the sensitivity, specificity and dynamic range to detect carotenoids in algae cells, experiments were conducted to confirm the co-localization of carotenoid in the lipid bodies using the Nile Red dye. Five major spectral components were extracted from hyperspectral images of Nile Red labeled algal cells (figure 2). Two spectral components associated with Nile Red were detected: fluorescence in which the Nile Red is bound to the neutral lipid (i.e. TAG) and fluorescence resulting from the Nile Red being bound to phospholipid. A spectral component that is representative of the carotenoid present in algal cells and highly similar to the mean spectrum is depicted in the figure 1. A component assigned to the chloroplast consisted of Chl-*a* as well as carotenoid spectral features. Typically it is desirable to spectrally separate each emitting species, however since chlorophyll is highly co-located with carotenoid within the thylakoids of the chloroplast (given

the diffraction limited spatial resolution), MCR cannot spectrally separate the two components. For the purposes this study, this is a desirable result since the primary interest is in identifying a spectral component that distinguishes the chloroplast features of the cell relative to the lipid bodies. Finally, an autofluorescence spectral component that correlated to the physiological state of the algal cell was also identified. Although this signal was spatially diffuse, the signal intensity was found to increase with the age of the culture and in the simulated culture crash, and varied inversely with the intensity of the chlorophyll within the cells.

In addition to the spectral components, MCR can also be used to calculate the concentrations (or intensities) of each spectral component for each voxel (volume-pixel) in the images. These concentrations can be reconstructed to produce the concentration images on a per component basis. These concentration images were used to construct RGB images that are instructive in showing the spatial relationship of the spectral components within each image. Figure 3a shows an RGB image of the carotenoid spectral component (red) and the chloroplast component (green). The chloroplast is varying shades of yellow/green due to the colocation of the carotenoid spectral component with the chloroplast spectral component, whereas in the lipid, the only fluorescing species is due to carotenoid, therefore the droplets show up as being pure red in the RGB image. Unfortunately, no endogenous fluorescence component associated with the extracellular matrix of the algal cell was observed; therefore it is difficult to ascribe the spatial relationship of the lipid and chloroplast to the overall location within the algal cell. An RGB image was used for comparison with the concentration image of the Nile Red (TAG) spectral component to confirm that carotenoid is located in the lipid droplet (figure 3b). However, one of the major challenges with the use of Nile Red to stain TAG is that it must first permeate the extracellular matrix in order to stain the lipid. Therefore, the effectiveness of Nile Red is dependent on the permissibility of the cellular bodies to the dye, leading to variability in the staining of the lipid. This effect can be seen clearly in figure 3b, where some of the droplets have much more Nile Red fluorescence intensity than others in spite of the overall size, whereas the carotenoid fluorescence in the droplets is more evenly distributed.

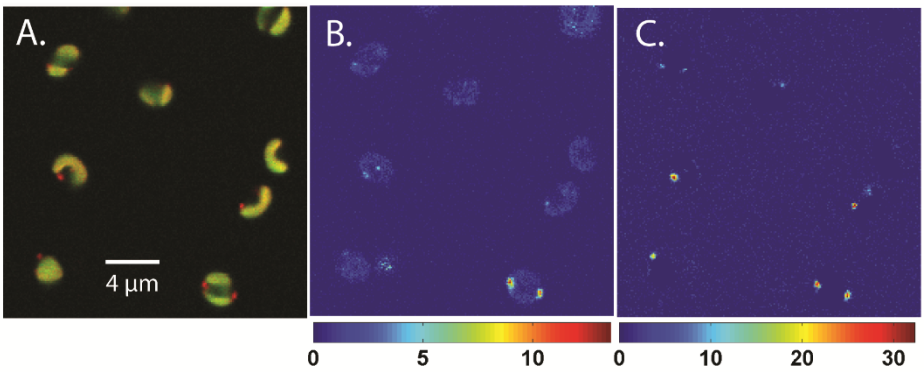

Figure 3. Images of *Nannochloropsis sp.* cells from the Nile Red staining experiment. (A.) An RGB image constructed using the concentrations from the chloroplast (green) and carotenoid (red) components. The chloroplasts are varying shades of green/yellow due to the components being colocated in the pixels; however the carotenoid component is only present in the lipid droplets. (B.) Concentration image of Nile Red TAG component showing the magnitude and location of intensities. (C.) Concentration image created using the label-free methodology using the carotenoid signal.

As explained above and shown in figure 1, the carotenoid emission co-exists in both the chloroplast and the lipid, therefore additional spectral features were required to separate the signals and produce quantitative images of the lipid and chloroplast bodies. Differentiating factors that allowed unequivocal identification of the chloroplast and the lipid bodies include a distinct fluorescence envelope and altered relative intensities of the resonance-enhanced Raman bands in the chloroplast compared to the lipid bodies. Furthermore, since chlorophyll *a* co-varies with the carotenoid present in the chloroplast, significant contributions from chlorophyll *a* fluorescence emission are also observed.

2.3. *Label-free evaluation of nutrient depletion-induced lipid accumulation*

A temporally dependent nutrient depletion study was used to investigate the effects of physiological changes relevant to photosynthetic productivity and lipid accumulation in *Nannochloropsis*. The experimental design included a wide range of initial nitrate and bicarbonate concentrations (see conditions 1-4 in the methods section) to assess the sensitivity of the physiological effects to varying nutrient conditions, and allows comparison of the label-free approach with numerous previous reports on the topic of nutrient deprivation-based lipid enrichment in alga. Daily imaging experiments were performed on algae cells from culture in mid-log phase (day 0) through onset of senescence (day 16). The individual spectral components from MCR analyzed data are very similar to the pure components obtained in the previously described Nile Red experiments (figure 4A). Quantitative interpretation of the lipid and chloroplast signals was made based on 3D rendered volumes, examples of which are provided in Figure 4b. In addition to volumetric data, the images provide novel insights into potential biological mechanisms of lipid accumulation based on the size and spatial orientation of the lipid bodies respective to the chloroplast. In the majority of cases, lipid bodies appeared in the close vicinity of the chloroplast and in many cases appeared to be directly coupled to the long axis of the ovoid chloroplasts via a thin stalk. This observation is suggestive of direct materials transfer between the chloroplast and the lipid body, likely through transient tubules known as plastid stromules (Hanson & Sattarzadeh, 2011), analogous to previous reports in *Chlamydomonas rheinhardtii* (Goodson et al., 2011). Previous studies have shown that plastid stromules have a functional role for connecting individual plastids, and support transfer of proteins between neighboring organelles in higher plants (Kohler et al., 1997). Furthermore, the size of the individual lipid bodies rarely exceeded the initial size of the neighboring chloroplast, and in several cases strings of adjacent, similarly-sized lipid bodies were detected. These observations are indicative of controlled dynamics that may include an active role for lipid bodies in lipid homeostasis, including oil synthesis and degradation, as was recently suggested based on proteomic analysis of lipid bodies from nitrogen deprived *Chlamydomonas rheinhardtii* (Nguyen et al., 2011). Figure 4c depicts the temporal evolution of the lipid body and chloroplast volumes and the corresponding volumetric ratios. Consistent trends were observed for each of the nutrient conditions, including dramatic increase in lipid fraction of the cell over the course of the experiment (Fig 4a). The percent lipid ranged from ~10 % at log phase (days 0-3) to ~50% (days 13-16). A correlated decrease in the chloroplast volume with increasing lipid is also clearly indicated (fig 4b). Figure 4c summarizes the results by showing the ratio of the lipid volumes to chloroplast volumes. The result is indicative of an apparent stoichiometric volumetric exchange between the lipid bodies and the chloroplast, and is highly conserved under a wide range of nitrate (1.55 - 21.55 mM) and bicarbonate (2.1 – 7.1 mM) initial conditions.

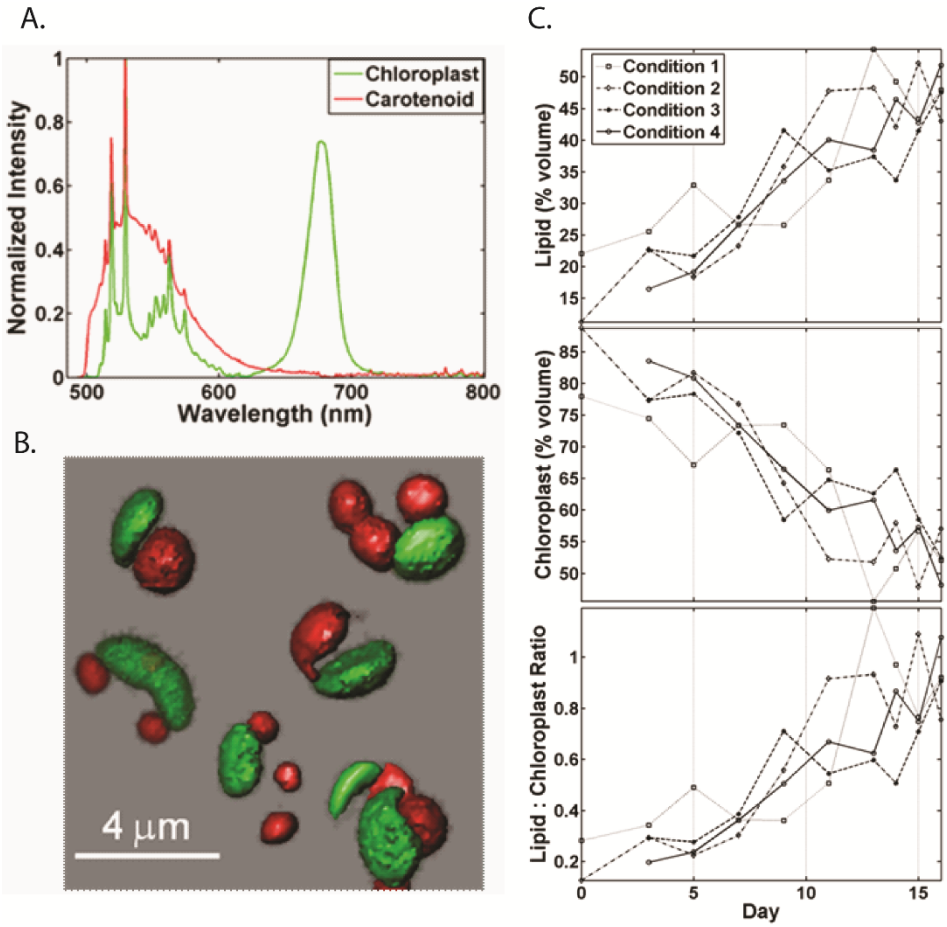

Figure 4. (A.) Pure component spectra from the temporally-dependent experiment to identify nutrient depletion effects on lipid production. (B.) Representative data of label-free RGB rendered 3D images of *Nannochloropsis* during nutrient deprivation. Red represents the volume of the lipid droplets (as indicated by carotenoid) and green represents the volume of the chloroplast. Percent volumes of the lipid and chloroplast using the total volume calculated from the summed components. (C.) Percent lipid volume plotted as a function of the growth condition replicate and day of experiment (top). Percent chloroplast volume (middle). The ratio of the percent lipid and chloroplast volumes (bottom).

Two distinct TAG synthesis pathways have been identified in algae, *de novo* synthesis, also known as the Kennedy pathway, and a lesser understood membrane recycling pathway (for a recent review, see (Chapman & Ohlrogge, 2012) and the references therein). The Kennedy pathway uses diacylglyerol acyltransferase (DAGAT) in an acyl-CoA dependent reaction to generate TAG from diacylglycerol (DAG). During membrane recycling, phospholipid: diacylglycerol acyltransferase (PDAT) is used for transacylation between phospho- and galactolipids and DAG, as well between two DAG equivalents, to produce TAG independently of acyl-CoA (Dahlqvist et al., 2000; Yoon et al., 2012). From a biophysical perspective, the chloroplast is primarily composed of an extended manifold of membranes with high effective surface area to support energy production via photosynthetic charge separation across the thylakoid. In light of this, our observation of a nearly quantitative exchange of the volume

fraction from chloroplast to lipid body strongly suggests that the membrane recycling mechanism is dominant in nutrient deprivation-based lipid accumulation in *Nannochloropsis sp*. Recent work using the model algae *Chlamydomonas rheinhardtii* both corroborates this assessment and ascribes additional lipid-related metabolic functionalities to PDAT, suggesting that PDAT-mediated membrane recycling may be a highly conserved mechanism among microalgae (Yoon et al., 2012).

2.4 Label-free classification of outdoor algae cultures and a simulated culture crash

The scatterplot shown in Figure 5 illustrates the ability to classify an outdoor pond with respect to lipid production and the health of the cells. Week 1 (red points) shows healthy cells with increased chlorophyll. Week 2 (green points) shows cells becoming stressed (lower chlorophyll) with increased lipid lipid production. After the hypochlorite-induced pond crash, the majority of the cells fall in the upper right hand quadrant with an increase and dominance in the autofluorescence. Together, these three spectral biomarkers can be used to describe two of the most important parameters in algae cultivation: 1) lipid production rates and 2) health degradation of the pond or raceway.

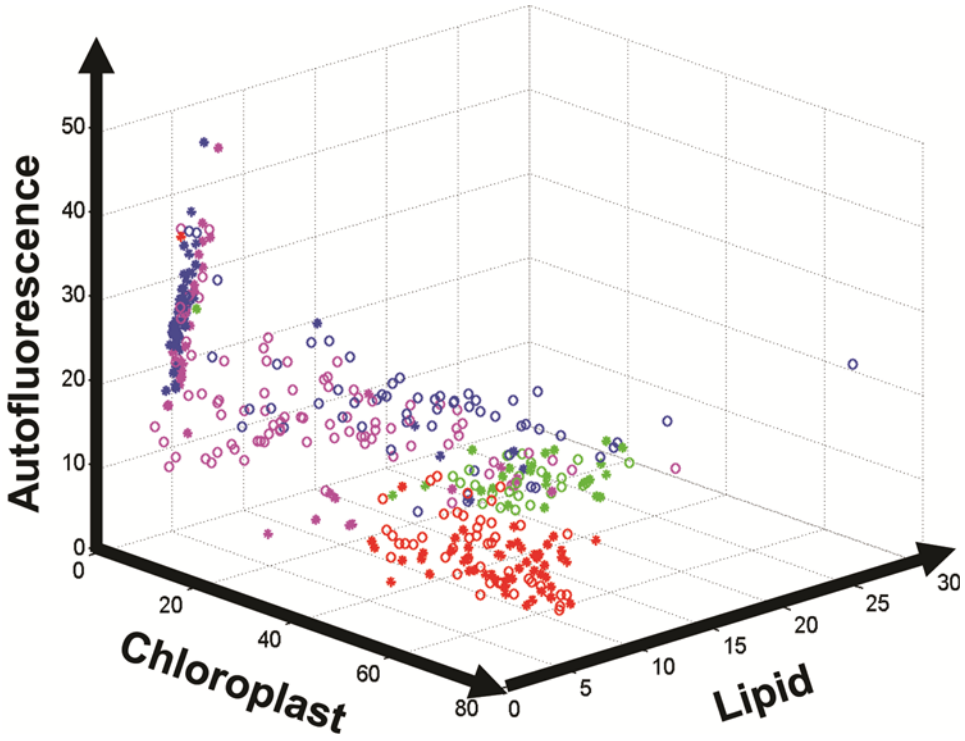

Figure 5. Classification of *Nannochloropsis sp.* grown in outdoor cultures using spectral signatures identified using fluorescence hyperspectral imaging and multivariate curve resolution. Scatter plot of the 3 spectral signatures (● - west pond, ○ - east pond). Red markers indicate mean concentrations after one week of culture; green markers indicated mean concentrations after two weeks of culture; blue markers indicate mean concentrations one day after a simulated culture crash; and magenta markers indicate mean concentrations two days after a simulated culture crash.

3.1 Multimodal Algae Bioprospecting

Among the issues facing the algae bioproducts industry, the lack of efficient means of cultivar screening and phenotype selection represents a critical hurdle for rapid development and diversification. To address this challenge, we have developed a multi-modal and label-free optical tool which simultaneously assesses the photosynthetic productivity and biochemical composition of single microalgal cells, and provides a means for actively sorting attractive specimen (bioprospecting) based on the spectral readout. The device integrates laser-trapping micro-Raman spectroscopy and pulse amplitude modulated (PAM) fluorometry of microalgal cells in a flow cell. Specifically, the instrument employs a dual-purpose epi-configured IR laser for single-cell trapping and Raman spectroscopy, and a high-intensity VIS-NIR trans-illumination LED bank for detection of variable photosystem II (PSII) fluorescence. Micro-Raman scatter of single algae cells revealed vibrational modes corresponding to the speciation and total lipid content, as well as other major biochemical pools, including total protein, carbohydrates, and carotenoids. PSII fluorescence dynamics provide a quantitative estimate of maximum photosynthetic efficiency and regulated and non-regulated non-photochemical quenching processes. The combined spectroscopic readouts provide a set of metrics for subsequent optical sorting of the cells by the laser trap for desirable biomass properties, e.g. the combination of high lipid productivity and high photosynthetic yield. Thus the device provides means for rapid evaluation and sorting of algae cultures and environmental samples for biofuels development. This work was published in Davis et al. *Proceedings of SPIE* 2014 and will be briefly summarized here (Davis et al., 2014b).

3.2. Simultaneous acquisition of Raman spectra and photosynthetic yield from algae cells

The process of evaluating and sorting cells requires basic coordination of hardware and software. In the initial state of the device, the trapping laser is "on" and the rapid light scanning pulse amplitude modulated (RLS-PAM) actinic LED is at low intensity. Dark adapted algal cells are fluidically transported from the syringe pump to the microfluidic chip containing the optical probe volume. The flow rate of the microalgae suspension depends on the concentration of the cells in the medium, however optimization of the flow velocity did not significantly improve the overall through-put of the device unless the sample was very dilute. In the probe volume, an individual cell is captured in the IR beam and illuminated by the RLS-PAM actinic LED, resulting in a chlorophyll fluorescence signal at the photodiode. The flow is then suspended via triggering based on an increase in the output of the photodiode of >10x background. The optical trap positions the cell several micrometers from the walls of the microfluidic well to avoid interfacial perturbations. Signals from regions outside the sample point are rejected by the confocal pinhole, affording high signal-to-noise ratio needed for single-cell Raman spectroscopy. Typical acquisition times for well-resolved spectra of algal cells were found to be ~10 s. Because lipid characterization relies on static accumulation of the Raman scattering signal and photosynthetic characterization relies on a temporally variable fluorescence response to intensity modulated excitation, the minimum total time scales of the two measurements allow a two-level photosynthetic yield assessment. For this assessment, fluorescence intensity data is collected at the low photon flux excitation (50 μmol/m^2/sec, 1 sec) followed by a saturation excitation pulse

(15000 µmol/m^2/sec, 1 msec), a subsequent increased photon flux excitation (1000 µmol/m^2/sec, 4 sec) followed by a second saturation excitation pulse, and a final low photo flux excitation (50 µmol/m^2/sec, 4 sec) followed by 1 sec exposure to the far red LED. After the 10 sec combined optical interrogation, the data is processed and the cell is retained or rejected based on user-defined parameters and actuated by the combination of galvo-based deflection of the laser and resumption of fluid flow.

Analysis of the micro-Raman data was performed using the ratiometric methods described in Wu, et al (Wu et al., 2011) for quantitative analysis of degree of unsaturation, carbon chain length, and phase transition temperature (T_m) of the cellular lipids. Briefly, the method uses the linear correlation between the intensities of the 1650 cm^{-1} (I_{1650}) and 1440 cm^{-1} (I_{1440}) to establish the number of degrees of unsaturation, the ratio of saturated and unsaturated carbons, and the T_m based on the the model lipid library described above. Multiplication of the values obtained for degree of unsaturation and ratio of saturated to unsaturated bonds provides the overall carbon chain length. Ratiometric comparison of the I_{1440} and the I_{1007} provides an additional estimate of the total lipid:protein for each cell.

Analysis of the RLS-PAM data for estimation of maximum photosynthetic yield, photosynthetic energy utilization, and regulated and unregulated photochemical quenching parameters was performed as described previously using the Stern-Volmer approach (Kramer et al., 2004; Schreiber, 2004). Briefly, under dark adaptation conditions, the average fluorescence intensity obtained under the initial (1 sec) low photon flux excitation provides the dark fluorescence yield (F_0). The maximum fluorescence yield (F_m) is obtained from the fluorescence plateau obtained during the brief saturation pulse. The maximum PSII quantum yield (F_v/F_m) is obtained from the equation,

$$F_v/F_m = (F_m - F_0)/F_m .$$

Following the initial PAR exposure, the subsequent elevated photon flux excitation provides the effective PSII quantum yield, *Y(II)*, obtained by the previous expression, with $F_m = F_m'$, ie. the modified F_m obtained at the fluorescence plateau during the second saturation pulse, and $F_0 = F$, ie. the modified F_0 obtained under increased, physiologically relevant PAR intensity (50-1600 µmol/m^2/sec photon flux). The non-photochemical quenching parameter, *NPQ*, is calculated according to a diffusion-limited Stern-Volmer quenching mechanism using the aforementioned fluorescence parameters according to the equation,

$$NPQ = (F_m - F_m')/F_m' .$$

The effective PSII quantum yield, *Y(II)*, sums to unity with the regulated, *Y(NPQ)*, and unregulated, *Y(NO)*, energy dissipation mechanisms to account for the PAR absorption in PSII. The coefficient of photochemical quenching, *qL*, required for differentiation of the two energy dissipation mechanisms is obtained following exposure to the far red illumination to obtain the

minimal fluorescence yield, F_0', and the aforementioned effective PSII quantum yield parameters according to the equation,

$$qL = F_0'(F_m' - F)/(FF_m' - FF_0')$$

Finally, *Y(NO)* and *Y(NPQ)* are calculated using the following equation, and by incorporating the unity constrain among these parameters and *Y(II)*.

$$Y(NO) = (1 + NPQ + qL(F_m/F_0 - 1))^{-1}$$

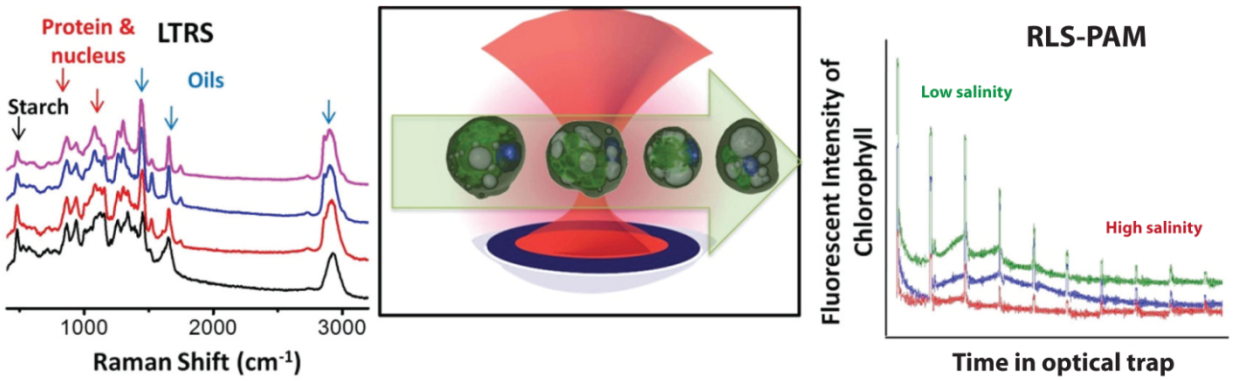

Figure 6. Simultaneous collection of Raman spectra and PSII yields from single laser-trapped algae cells cultured in media of varying salinity.

3.3 Identification of algal adaptation states with elevated productivity and lipid yield

In order to assess the sensitivity of the apparatus to the abiotic factors impacting the combination of photosynthetic and lipid productivities, the multispectral sorter apparatus was tested using monocultures of the common micoralgal production strain, *Dunaiella salina*, cultured at a range of salinities from ~0.5M to 2.5M. Because of the species' importance for nutraceutical and feed applications (Ben-Amotz & Avron, 1982; Moulton et al., 1987), *D. salina* provides a well-studied model for microalgal bioprospecting. Most important for this application, *D. salina* exhibits the somewhat remarkable property of increased photosynthetic yield (Liska et al., 2004) and a correlated increase in elongated and unsaturated lipids under high salinity regimes (Azachi et al., 2002).

Figure 7 depicts correlations among the major measured parameters for ~50 individual cells from each culture condition. In figure 4(A), average lipid carbon chain lengths and degree of unsaturation of the lipids is shown for the various salinity regimes. At the low salinity regime, the average carbon chain length was 16.07, variance 0.367; at the medium salinity regime the average was 16.32, variance 0.444; and at the high salinity regime the average was 16.38, variance 0.496. At the low salinity regime, the average single cell degree of lipid unsaturation was 1.24, variance 0.013; at the medium salinity regime the average was 1.55, variance 0.038;

and at the high salinity regime the average was 1.68, variance 0.083. To our knowledge this is the first report indicating increased cell-to-cell variance in the carbon chain length (135%) and degree of lipid unsaturation (638%) at increasing salinities in *Dunaliella salina*. In figure 4(B), the total lipid to protein ratio is plotted against the single-cell maximum (dark adapted) photosynthetic yield. At the low salinity regime, the maximum photosynthetic yield (F_v/F_m) was 56.6%, variance 0.0102%; at the medium salinity regime the F_v/F_m was 58.0%, variance 0.0095%; and at the high salinity regime the F_v/F_m was 60.9%, variance 0.0080%. At the low salinity regime, the lipid:protein was 1.67, variance 0.09; at the medium salinity regime the lipid:protein was 0.438, variance 0.047; and at the high salinity regime the lipid:protein was 0.91, variance 0.065. From this plot a correlation between high lipid:protein and reduced photosynthetic yield is apparent, although several outliers with simultaneously high lipid:protein and photosynthetic yield were detected. Furthermore, the single cell correlations between the photosynthetic yield and lipid:protein appear to provide reasonably high fidelity classification for the salinity adapted state of the cells.

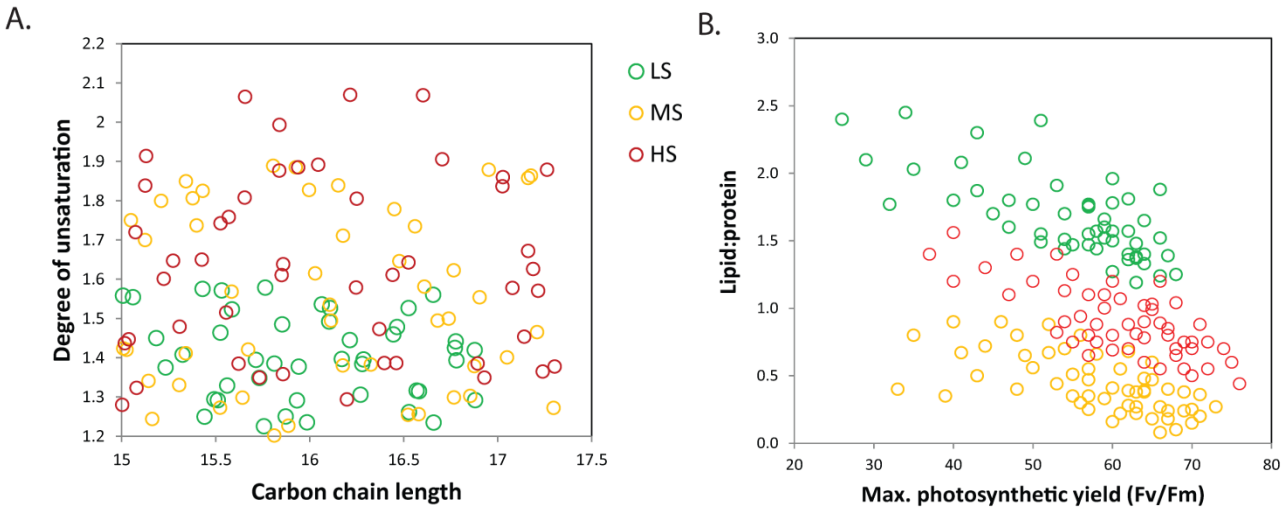

Figure 7. Single-cell parameters obtained from the multispectral sorter apparatus. A) Correlation between fatty acid carbon chain length and degree of unsaturation for *D. salina* cultivated at various salinity regimes (LS: low salt, MS: medium salt, HS: high salt). B) Correlation of the maximum photosynthetic yield and lipid:protein obtained from RLS-PAM and LTRS, respectively.

4.1 Semi-continuous culture and osmotic lipid particle release

Although great efforts have been made to elucidate the phenotypic responses of alga to varying levels of nutrients, osmotic environments, and photosynthetically active radiation intensities, the role of interactions among these variables is largely nebulous. Here we describe a general method for establishing and maintaining semi-continuous cultures of the halophilic microalgal production strain, *Dunaliella viridis*, that is independent of variations in salinity and illumination intensity. Using this method the cultures were evaluated to elucidate the overlapping roles of photosynthetic and osmotic adaptation on the accumulation and compositional variation of the biomass, photosynthetic productivity, and physiological biomarkers, as well as spectroscopic and morphological details at the single cell level. Correlation matrices defining the relationships among the observables and based on variation of the illumination intensity and salinity were constructed for predicting bioproduct yields for varying culture conditions. Following maintenance of stable cultures for six week intervals, phenotypic responses to photo-osmotic drift were explored using a combination of single cell hyperspectral fluorescence imaging and flow cytometry. In addition to morphological changes, release of lipid microparticles from the cells that is disproportionate to cell lysis was observed under hypotonic drift, indicating the existence of a reversible membrane permeation mechanism in *Dunaliella*. This phenomenon introduces the potential for low cost strategies for recovering lipids and pigments from the microalgae by minimizing the requirement for energy intensive harvesting and dewatering of the biomass. The results should be applicable to outdoor culture, where seasonal changes, resulting in variable solar flux and precipitation and evaporation rates are anticipated. These results were published in Davis et al *Journal of Applied Phycology* 2014 and will be briefly summarized here (Davis et al., 2014a) .

4.2 Phenotypic and compositional variation of D. viridis under varying photo-osmotic regimes

Dunaliella viridis cells cultured in the various photo-osmotic conditions were characterized using confocal fluorescence hyperspectral imaging to couple the compositional variation and photosynthetic and biochemical indicators with spectroscopic signatures and spatial data, including cell size and morphology. Figure 8 provides representative images (A) and a corresponding set of spectrally unmixed fluorescence components (B) obtained from batch processing of the aggregated imaging data using MCR. The intensity images in figure 8A were generated according to the relative abundance of the spectral components shown in figure 8B. Two distinct spectral features dominate the emission spectrum for all of the *D. viridis* imaging data, denoted as ‘chloroplast’ and ‘carotenoid’ in figure 8B. The chloroplast spectral component (green) is characterized by a high intensity Chl-*a* photosystem emission (peak at ~680 nm) colocalized with low levels of carotenoid emission; the carotenoid spectral component (red) is characterized by a minor, but broad chlorophyll fluorescence (~660-680 nm) with high levels of carotenoid emission (~520-600 nm). The sharp peaks within these spectra are not due to noise; instead they are a result of resonance enhanced Raman scattering. Typically, Raman bands would not be observed in a fluorescence measurement; however, resonance enhancement arising from absorption of the excitation laser near the electronic transition of the carotenoids is sufficient to amplify a subset of Raman-active modes by several orders of magnitude (Davis et al., 2013; Robert, 1999b). Specifically, these bands were assigned to three major vibrational modes of carotenoids, the C=C stretch (1529±10 cm^{-1} or 527 nm), the C-C stretch (1157±10 cm^{-1}

or 519 nm), and a C-C bend (1004±10 cm^{-1} or 514 nm). Although progressive shifts in the wavenumber of the C=C stretching band are correlated to increased polyene chain length, deviations in the exact frequency shift should be expected by interactions with the host matrix (de Oliveira et al., 2010). In addition to providing indication of the relative abundance and cellular localization of these spectral components, the data also provide an estimate of cell size and granularity for subsequent data interpretation.

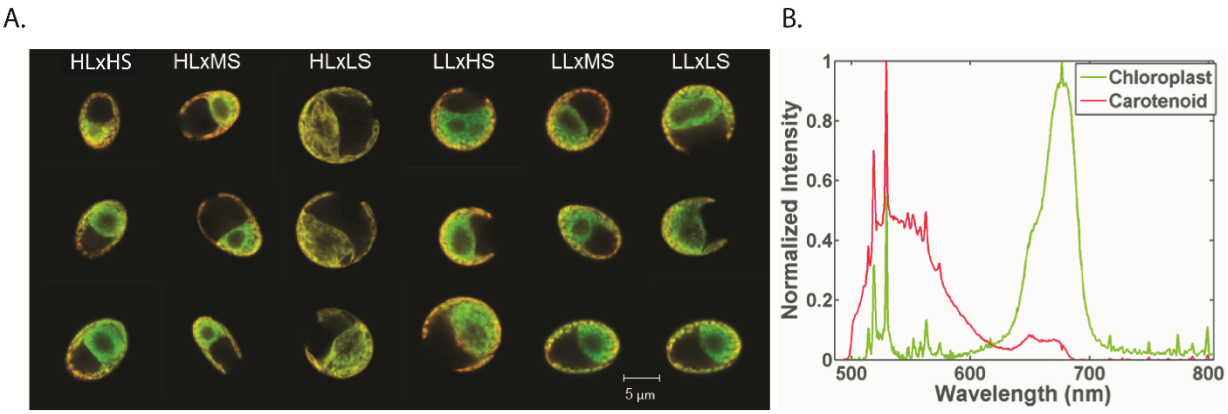

Figure 8. Hyperspectral confocal fluorescence images of *D. viridis* adapted to a variety of photo-osmotic conditions. A.) Representative hemispherical sections of individual *D. viridis* cells depicting phenotypic variations dictated by the various salinity and PAR illumination regimes. B.) Fluorescence emission components obtained by MCR analysis and used for intensity mapping of the cells depicted in part A.

Semi-continuous harvesting of the *D. viridis* biomass at log phase was achieved using a calibration data set collected from initial cultures representing each condition in the photo-osmotic adaptation matrix. Combining cell counts with the effective cell diameters obtained from fluorescence imaging data allowed prediction of the total biomass from the bulk spectrophotometric data. Correlation of the haemacytometry and flow cytometry data yielded nearly identical total cell counts (data not shown), however the standard deviation values of the haemacytometry data was significantly higher, therefore flow cytometry was chosen as the method of choice for linear regression analysis with VIS-NIR. The correlation between the near IR attenuation and cell counts obtained from flow cytometry for each of the serially diluted cultures. For all conditions tested $R^2 > 0.99$ were obtained, however, significant differences were observed in the slopes of the various culture conditions, indicating significant differences in the optical attenuation profile of the cells. Examination of the extrema of the near IR attenuation per cell (viz. HLxMS and HLxLS) suggest that the cell count predicted by the 800 nm optical densities varies by up to ~300% based on physiological changes introduced by the combination of salinity and PAR intensity investigated here. This deviation in the near IR attenuation per cell is nearly identical to the ratios of cell volumes observed from the confocal microscopy studies. In figure 2B the volume of the native (hydrated) biomass was calculated by multiplying the cell counts with the average cell volumes and correlated to the near IR attenuation for the undiluted log-phase cultures. In this case, regression analysis indicates a linear trend for an increasing volume fraction of the biomass with increasing 800 nm optical density (R^2=0.946). Together

these data suggest that despite substantial differences in cell size and biochemical composition, near IR attenuation is nonetheless a consistent indicator for total biomass accumulation. A primary implication of this finding is that water content in the cells is largely invariant despite the aforementioned biochemical and morphological differences. This finding is corroborated by measurements of AFDW of the aggregated samples (see Table 2). It is noteworthy, however, that the HLxHS culture deviates somewhat from the general trend observed in the other culture conditions. Specifically, *D. viridis* cultured under these conditions shows generally higher near IR attenuation per unit biomass, likely linked to increased pigment absorptions in this spectral region. Comparison of these data to calculations of the Mie scattering profile of a simplified microalgae model (Quirantes & Bernard, 2004) based on the observed variations in the effective cell diameters predicts a 180 – 240% increase in the near IR scattering profile over a refractive index difference range of 0.06 – 0.26. Comparison of these calculated changes with respect to the experimentally observed ~300% increase in near IR attenuation suggests that diffuse scatter is responsible for ~60 – 80% of the observed optical attenuation at 800 nm.

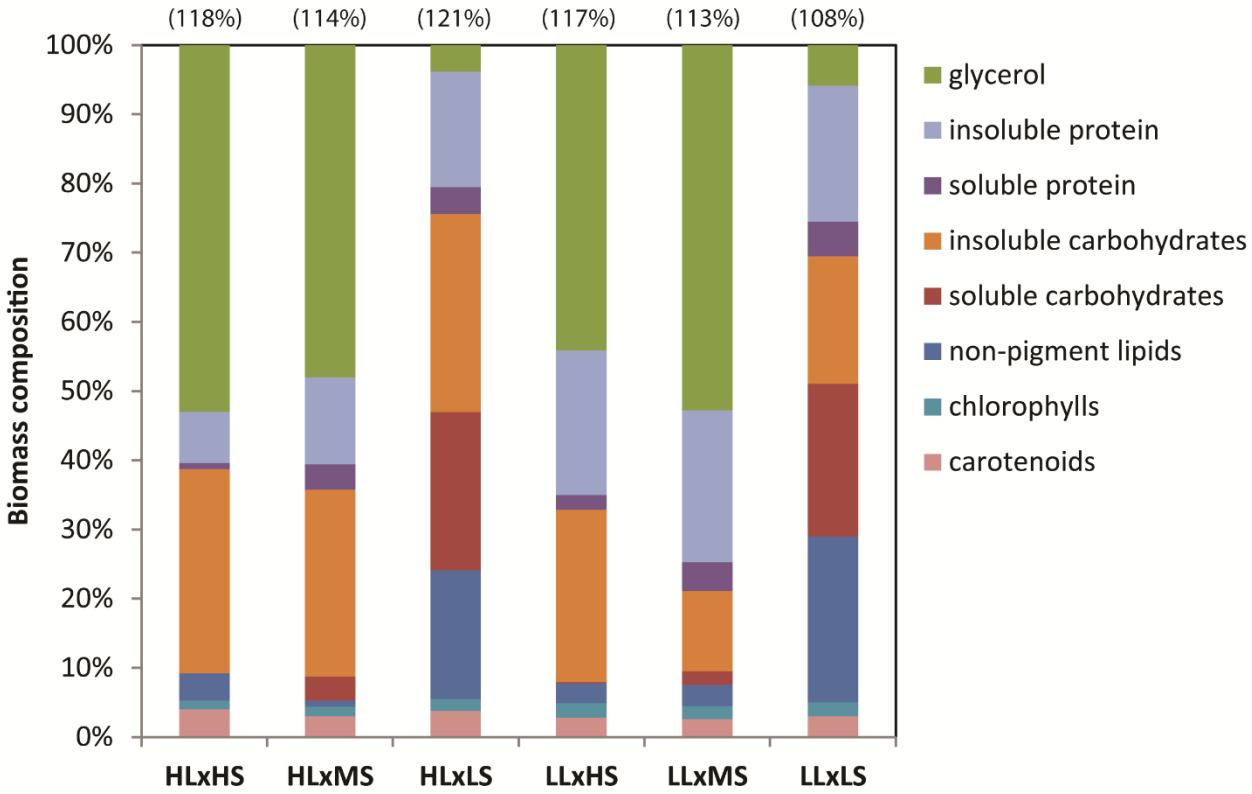

Figure 9. Mass balance of the dry weight of semi-continuous cultures of *D. viridis* in each of the photo-osmotic conditions. Overestimation of the AFDW mass balance for the pooled biomass samples (n=20 per condition) are depicted in parenthesis above the results obtained for each culture condition.

The compositional mass balance of the major biochemical pools of the biomass cultivated in the various photo-osmotic regimes are depicted in figure 9. The most significant compositional variations were observed in the quantities of glycerol, followed by soluble carbohydrates and (non-pigment) lipids. For each of the observed compositional shifts, the dominating environmental variable was change in salinity, with the largest effects predicated by shifts to or from low (marine) salinity levels. The total glycerol corresponded to 53-47% for high salt (~2.36 M NaCl), 52-47% for medium salt (~1.36 M), and 4-6% for marine medium. The soluble carbohydrates corresponded to <1% for high salt, 3-5% for medium salt, and 22-24% for marine medium. The non-pigment lipid fraction corresponded to 3-5% for high salt, 2-5% for medium salt, and 18-23% for marine medium. The most dramatic shifts that were dominated by light intensity levels were insoluble protein and insoluble carbohydrate, although substantial changes were also observed for chlorophyll (a+b) and carotenoids, despite their low abundance relative to the other fractions. The insoluble protein fraction corresponded to 8-15% for high PAR and 14-18% for low PAR. The insoluble carbohydrate fraction corresponded to 28-30% for high PAR and 11-21% for low PAR. For each assessment of compositional mass balance, the summed mass fractions exceeded the mass of the biomass between 6 – 22%, indicative of some combination residual salts and cross-talk (additive noise) among the various measurements. Based on additive accumulation of error distributed among the various biochemical fractions, the approximate error for each fraction is <3%. For completeness, the overestimates relative to the measured dry weight of the biomass are stated in parenthesis above the data for each culture condition.

Photosynthesis parameters, including the maximum [Y^{max}(II)] and effective [Y(II)] quantum yields of PSII, and regulated (photo-protective) non-photochemical [Y(NPQ)] and unregulated non-photochemical quenching [Y(NO)] obtained from RLC excitation modulated fluorescence experiments are depicted in figure 10. The results are summarized for dark adaptation, at the 50 μmol photons m^{-2} sec^{-1} exposure – corresponding to the low light growth regime, and at the 275 μmol photons m^{-2} sec^{-1} – corresponding to the high light growth regime, respectively. For each data set, clear trends are evident and related to the specified growth condition, with the dominant effects dictated by changes in salinity. For the dark adapted state, Y^{max}(II) increased with elevated salinity and reduced light exposure from 59% (HLxLS) to 73% (LLxHS). Culturing at low light intensities consistently increased the maximum photosynthetic yield by ~5% compared to the corresponding high light cultures. At the low light exposure during the RLC, Y(NPQ) is significantly elevated relative to unregulated processes Y(NO) for cultures grown at reduced salinities and increased PAR. At the high light exposure during the RLC, the salinity dependence of Y(NPQ) relative to Y(NO) is dramatically reduced, although Y(NPQ) continues to be elevated by 1.2 – 2x for cultures grown at increased PAR. The highest Y^{max}(II) and Y(II) values were consistently observed in the low light, high salinity cultures, indicating enhanced overall photosynthetic productivity under the elevated salinity regimes.

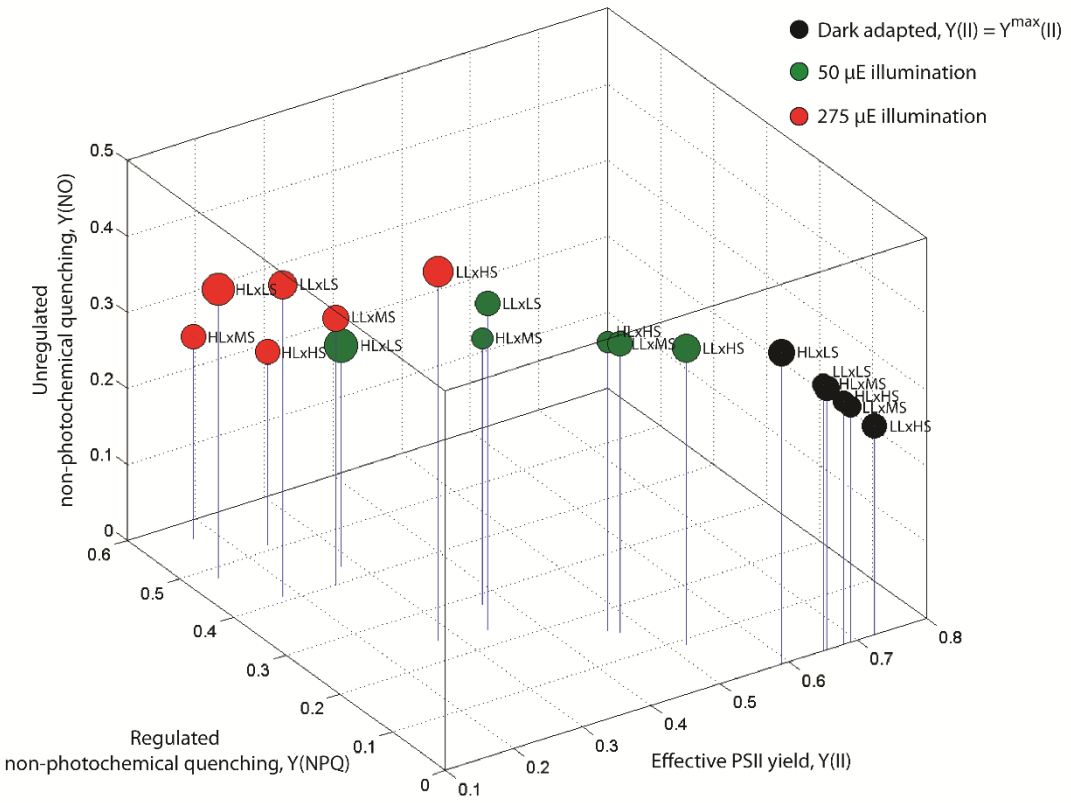

Figure 10. PSII parameters obtained for each of the culture conditions, including maximum PSII yield, $Y^{max}(II)$; effective PSII yield, Y(II); regulated non-photochemical quenching, Y(NPQ); and background or unregulated non-photochemical quenching, Y(NO). Data from dark adapted cultures are represented with black markers, low PAR (50 µE) illuminated samples with green markers, and high PAR (275 µE) illuminated samples with red markers. The marker sizes correspond to the 1σ standard deviation (n=20) obtained from the full data collection period.

4.3 Lipid particle release under osmotic drift

Following the six week semi-continuous culture and harvesting of *D. viridis* in the specified photo-osmotic culture conditions, each culture was subject to continued semi-continuous culture in either of the extreme of salinity (HS or LS) for additional harvesting cycles (8 days). The most noteworthy observation was made by comparing flow cytomery data of Nile Red stained cells at day 0, corresponding to the initiation of the dynamic osmotic adaptation regimen, to replicate experiments performed at the second harvest interval of the osmotic shock treatment (4 days after initiation of the regimen). Figure 11A and B depict scatter plots corresponding to effective particle diameter (FSC) and Nile Red intensity (FL2) for day 0 and day 4, respectively. These data clearly reveal a band of highly lipophilic microparticles ranging in diameter from ~1 – 3 µm in addition to the expected grouping of intact *D. viridis* cells. Comparison of Nile Red intensities per unit volume from each population suggests that the lipid concentration in the microparticles is up to ~1275% that of the algal cells. Figure 6C depicts the total lipid mass balance (as indicated by Nile Red intensity) of the lipophilic microparticles compared to the

remaining intact cells. In each case of cells semi-continuously cultured in decreasing salinity media, the total lipid was highly concentrated in the lipophilic microparticle phase, whereas in the cases of cells resuspended in increased salinity, the total lipid was primarily concentrated in the algae. The highest overall lipid was observed in MS cultures diluted by marine (LS) medium, however it is noteworthy that the high PAR culture (HLxMS) exceeded the low PAR culture (LLxMS) for total lipid by a factor of ~200%. Because other debris and instrumental background dominate the flow cytometric signal for particles less than ~1 µm in diameter, the contribution to the total lipid and the ratio of the lipid in the microparticles versus the intact cells should be treated as the lower bound of the estimates.

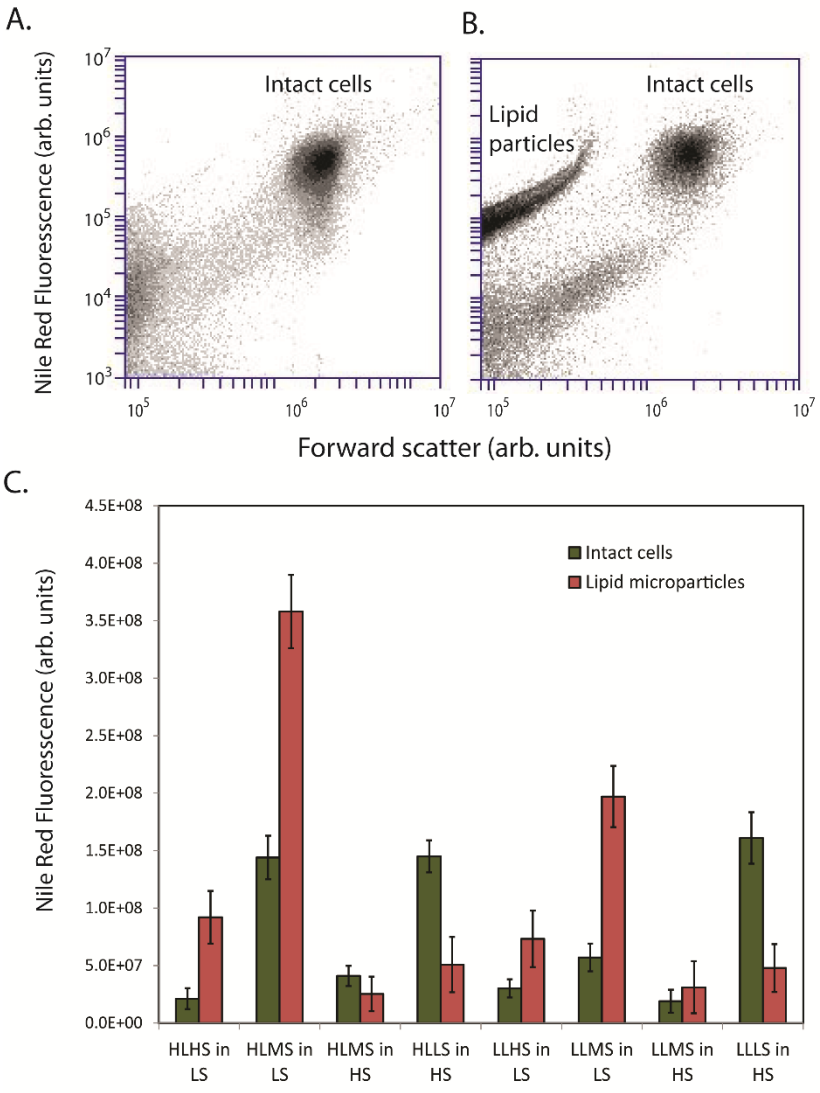

Figure 11. Lipid microparticle release under osmotic drift. A.) Flow cytometry scatter plot for total lipid (as indicated by Nile Red fluorescence intensity) versus particle diameter (as indicated by forward scatter) for the first day of osmotic shock in the HLxMS culture. B.) Repeat scatter plot for the fourth day of osmotic shock, corresponding to the second harvesting increment. C.) Summary of the total lipid content in the intact cell and lipid microparticles as indicated by Nile Red fluorescence, error bars indicate 1 σ standard deviations (n=3).

	HLxHS	HLxMS	HLxLS	LLxHS	LLxMS	LLxLS
			Biomass Yield (d^{-1})			
V_{cell} (μm^3)	252±72	280±89	696±132	366±111	335±106	414±125
N_{cells} ($x10^3$ mL^{-1})	1961±29	2982±37	370±24	1137±26	1345±33	173±27
Biovolume ($x10^{-4}$ mL^{-1})	4.94±0.28	8.37±0.33	2.58±0.25	4.17±0.33	4.52±0.34	1.71±0.46
Ash-free dry weight (g/L)	0.143±0.007	0.218±0.009	0.062±0.006	0.117±0.009	0.118±0.009	0.04±0.01
			Bioproduct Yield (fraction of dry weight)			
Carotenoids	0.044±.006	0.034±0.006	0.032±0.007	0.037±0.005	0.029±0.004	0.026±0.005
Chlorophylls	0.016±0.005	0.023±0.004	0.023±0.006	0.034±0.006	0.031±0.005	0.035±0.006
Lipids	0.11±0.03	0.09±0.03	0.23±0.05	0.11±0.03	0.10±0.03	0.26±0.03
Carbohydrates	0.31±0.04	0.34±0.05	0.55±0.06	0.27±0.05	0.19±0.04	0.46±0.05
Proteins	0.14±0.04	0.16±0.04	0.29±0.06	0.23±0.04	0.26±0.04	0.24±0.04
Glycerol	0.56±0.05	0.49±0.05	0.08±0.04	0.49±0.05	0.52±0.06	0.06±0.05
			Physiological Biomarkers			
Cell granularity†	1.55±0.14	1.63±0.18	2.78±0.22	1.02±0.09	1.13±0.10	2.23±0.18
Debris content	0.57±0.06	0.92±0.14	0.72±0.08	0.31±0.19	0.96±0.11	0.63±0.10
Motility	0.90±0.04	0.94±0.05	0.82±0.06	0.89±0.03	0.91±0.03	0.84±0.05
Int. pH	7.63±0.14	6.67±0.10	6.78±0.22	7.35±0.14	6.98±0.09	7.15±0.20
Ext. pH	9.20±0.04	9.27±0.05	9.11±0.06	9.19±0.04	9.06±0.06	8.82±0.08
Int. Ca^{2++}	3.73±0.28	1.64±0.26	3.2±0.31	3.81±0.26	2.33±0.22	3.57±0.30
Δ[NO_3] (mM)	1.45±0.12	1.08±0.14	0.937±0.19	0.741±0.14	0.788±0.09	0.821±0.11
ΔNAD(P)H^+	0.483±0.044	0.73±0.050	0.44±0.052	0.35±0.71	0.367±0.043	0.567±0.055
			Photosystem II Parameters			
Max yield, Y^{max}(II)	0.69±0.03	0.64±0.02	0.59±0.05	0.72±0.03	0.69±0.03	0.65±0.04
Low PAR yield, Y(II)	0.47±0.03	0.39±0.03	0.28±0.04	0.53±0.03	0.47±0.02	0.34±0.04
Low PAR Y(NPQ)/Y(NO)	0.47±0.21	0.72±0.19	1.48±0.23	0.21±0.13	0.43±0.18	0.56±0.12
High PAR yield, Y(II)	0.24±0.04	0.17±0.02	0.14±0.04	0.27±0.03	0.24±0.02	0.18±0.03
High PAR Y(NPQ)/Y(NO)	1.96±0.23	1.90±0.25	1.00±0.20	0.51±0.27	1.11±0.21	1.00±0.23

Table 1. Summary of the measured parameters obtained in assessment of the photo-osmotic adaptation matrix. Error values correspond to 1-σ standard deviations for each of the measurements. For AFDW and the bioproduct yields, the errors originate from 3 replicate measurements from biomass that was pooled from the 20 semi-continuous harvesting intervals. For the remaining parameters, n=20 per condition. Observables indicated by (†) are relative intensities obtained spectrophotometrically.

5.1 Algal Recalcitrance and Enzymatic Lysis

Comparison of mechanical and chemical pretreatments of *Nannochloropsis salina* and *Dunaliella salina* were performed to determine the relative recalcitrance of the two algae species. Initial studies were performed using vacuum filtration of freshly harvest biomass using 1 µm and 200 nm pore size filters. The results of this assay is depicted in figure 12. From these data, *D. salina* exhibits low structural recalcitrance. The bulk of the biomass is disrupted by shear forces during vacuum filtration for both pore sizes under all treatments. *N. salina* on the other hand exhibits high structural recalcitrance. For this species boiling dilute acid results in fragmentation of cells to generate particles <1 µm but >200nm in diameter. Based on these data, *Nannochloropsis* was chosen as the target species for subsequent enzymatic digestion assays.

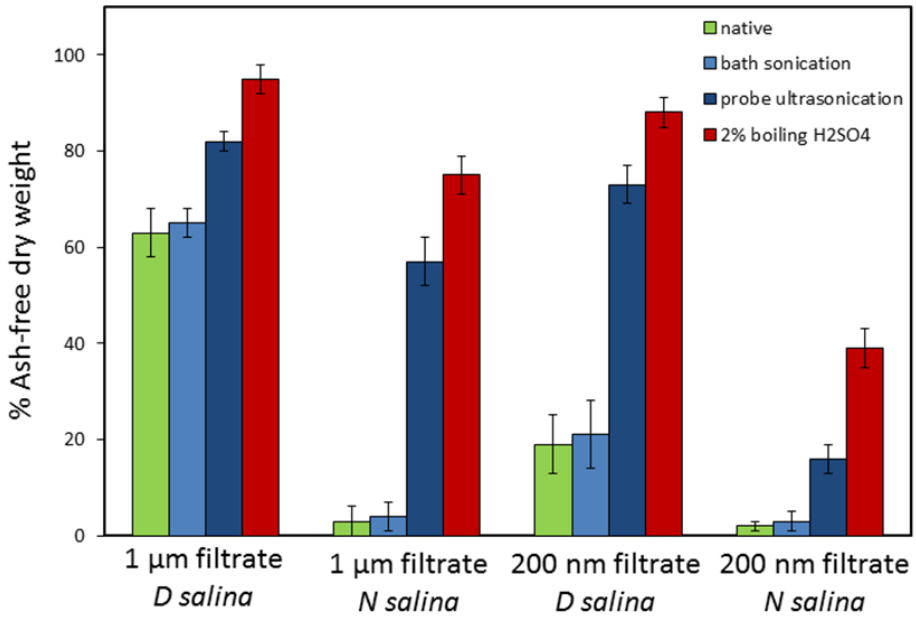

Figure 12. Comparison of structural recalcitrance of *Dunaliella salina* and *Nannochloropsis salina* by vacuum assisted filtration following bath sonication, probe ultrasonication, and dilute acid pretreatments.

A variety of enzymatic treatments were performed on Nannochloropsis biomass, including endoglucanases, cellobiohydrolases, β-glucanases, endoxyalanases, pectinases, and endopeptidases. Of particular interest for this application were halophilic enzymes originating from the prolifically cellulolytic fungi, *Aspergillus niger* and *Trichoderma reesei*; and natural predators of marine microalgae, especially *Aplodactylus punctatus* and *Helix pomatia*. The CAZy classifications for these enzymes included, endocellulase (EC 3.2.1.4), exocellulase (EC 3.2.1.91), β-glucosidase (EC 3.2.1.21), xylanase (EC 3.2.1.8), pectinase (EC 3.2.1.15), proteinase K (EC 3.4.21.64) (*Tritirachium album),* subtilisin (EC 3.4.21.62) (*Bacillus subtilis*), lysozyme (EC 3.2.1.17), and arylsulfatase B (EC 3.1.6.1) (*E. coli*). The relative activities of these enzymes following 24 hrs of exposure at 40C on a shaker incubator is depicted in Figure 13.

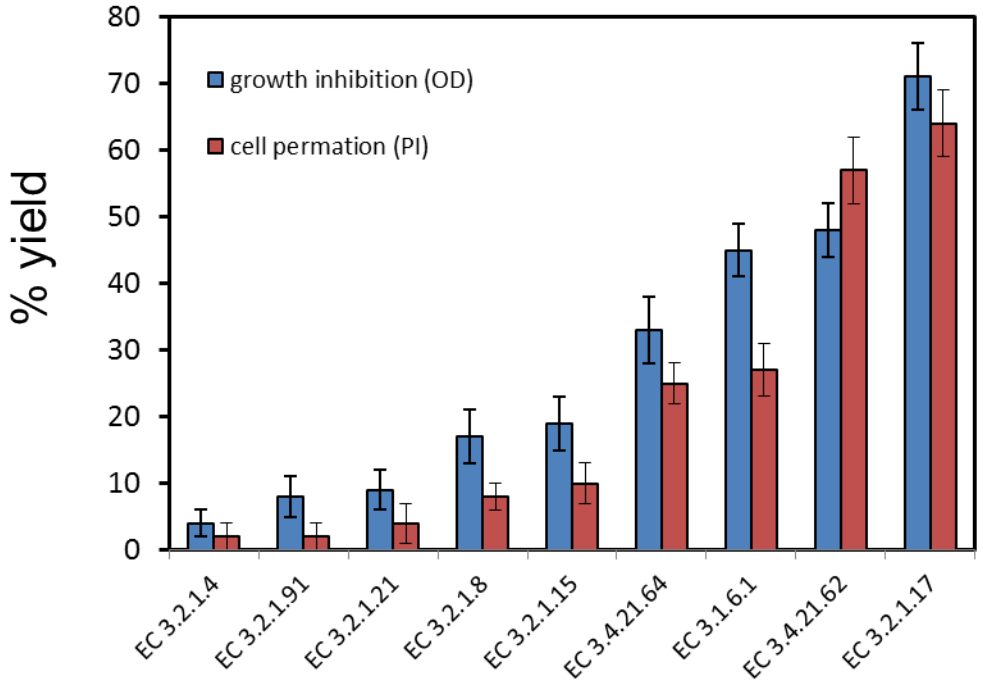

Figure 13. Enzymatic activity on live Nannochloropsis salina biomass as indicated by growth inhibition using NIR optical density (OD) and cell permenation using propidium iodied staining (PI).

In this assay growth inhibition and cell permeation were highly correlated as anticipated. The three best performing enzymes, lysozyme, aryl sulfatase, and alcalase, respectively. Lysozyme preferentially cleaves peptidoglycan bonds, indicating that protein-carbohydrate bonds are likely candidates for the structural integrity of *N. salina* cells. Aryl sulfatase preferentially cleaves sulfo-glycan bonds, indicating that sulfo-sugars are likely present in the algae cell wall. This is consistent with previous reports of sulfo-sugars in alga, which have been targeted as a potential bioproduct of algae with biomedical applications (Jiao et al., 2011). Alcalase is serine protease, further suggesting that proteins provide a significant structural contribution to recalcitrance in microalgae.

5.2 Genetic transformation of Nannochloropsis

The aforementioned best performing enzymes for deconstruction of *Nannochloropsis* were of highest priority for heterologous expression because of limitations in plasmid stability for introducing combinatorial plasmid-based modifications. Because expression of the stated heterologous gene products was known to be toxic to Nannochloropsis, we adopted the protocols developed for expression using a lipid droplen surface protein (LDSP) promoter targeted to nutrient-limitation based lipid accumulation and a 35S terminator sequence (Vieler et al., 2012). This approach targets algae production in batch culture, where nitrogen limitation is concomitant with onset of lipid production and peak biomass accumulation, thus preventing unwanted detriment to overall biomass productivity during active growth. Plasmids were assembled with

each of the individual enzymes and all three enzymes on a single plasmid. The DNA sequences and primers that were employed for PCR addition into plasmids are enumerated below.

35s AGTCCGCAAA AATCACCAGT CTCTCTCTAC AAATCTATCT CTCTCTATTT
TTCTCCAGAA TAATGTGTGA GTAGTTCCCA GATAAGGGAA TTAGGGTTCT
TATAGGGTTT CGCTCATGTG TTGAGCATAT AAGAAACCCT TAGTATGTAT
TTGTATTTGT AAAATACTTC TATCAATAAA ATTTCTAATT CCTAAAACCA
AAATCCAGTG AC

LDSP promoter AAGATGGAGT GGATGGAGGA GGAGGCCTCG GTGGCCGCTA
GCGTGTCGTA CACTGCTCGG CACATGAGCC AGAGCTTCGG CCTGGGGCTG
AAGATCCACG CCCTGATCAC TCTGGGTCAC GCCAAGAGCA ACGCCGAGGC
CCATCATACC AAGCGCTGCG TGGCGCGCTG CGGCCTGAAG CTGCACACCT
CGTAAAGCCC GCCCAAGGGC CTGGAGCGCC GGGACCCCCT GGCCTAGCCC
ATGCTGTTCG ATGCGGTGTG CTTCGTCACG GTGGATGTCA TTCAGGAGTC
CGGTGCGTGC CGCAGCTTCT TTTCCGCCTG ATACCGCTCC TTTCCGCTCC
GCACCATCCG GCCCCCCTTT CTGCCTCTGT GCGAGGGCGT GGGCGTCGCC
GTGCTGCTGT GCGGTCGCCA TCTGCGCTGG TAGCCCGCCT CCCGCCGCCT
GGTGGACGTC ACGAGCCTCT TTACCGTGCT CCGGCGCCGC GACGCCTCGG
AGACCGCTCT CGACCTGCTG GACACGCACT CGGTCTGCGA GCTCGTGGAC
TCCGACACGA CTTCGGAGAG CTCGCCGCTG CCTATGGTGC AGCTGCTGGT
GACCAAGTTC TGACTGCGGC GGTACCACCA CTCCCGCAGC TGCGCCTGGC
TCTTCCGCCA CGCGGGGCTC CCGCGCGGCG GCGCGATCTT CTAAAACCTG
ACGCAGAACA CCGCCCTGAC CCCCCACACC TATTCCTAGT AAACGACCAC
GAACCTGTCC CCCCACCAGC ACCGCCGCGC CCCGGGGGGC AACAAGATC

Sulfatase ATGAGCAAGC GCCCCAACTT TCTGGTGATT GTCGCGGACG ACCTGGGCTT
CAGCGACATC GGGGCGTTTG GCGGGGAGAT TGCGACCCCG AACCTGGACG
CTCTGGCCAT TGCCGGTCTG CGCCTGACTG ACTTCCACAC GGCTTCGACG
TGCAGCCCGA CCCGCTCGAT GCTGCTGACG GGCACCGACC ACCACATCGC
CGGCATTGGC ACCATGGCCG AGGCGCTGAC GCCGGAGCTG GAGGGCAAGC
CTGGGTACGA GGGTCATCTG AACGAGCGCG TGGTGGCGCT GCCCGAGCTG
CTCCGGGAGG CGGGCTACCA AACCCTGATG GCTGGCAAGT GGCACCTGGG
CCTGAAGCCG GAGCAGACCC CCCACGCCCG CGGCTTCGAG CGCAGCTTTT
CGCTGCTGCC CGGCGCCGCC AACCACTACG GCTTCGAGCC CCCCTACGAC
GAGTCGACCC CTCGCATTCT GAAGGGCACG CCCGCCCTGT ACGTGGAGGA
CGAGCGCTAC CTGGACACCC TGCCCGAGGG GTTCTACAGC TCGGACGCCT
TCGGGGACAA GCTGCTGCAG TACCTGAAGG AGCGGGACCA ATCGCGCCCG
TTCTTCGCGT ACCTGCCGTT CTCCGCCCCG CACTGGCCCC TCCAGGCGCC
CCGCGAGATC GTGGAGAAGT ACCGGGGCCG CTACGACACC GGCCCTGAGG
CTCTGCGCCA GGAGCGCCTG GCTCGGCTGA AGGAGCTGGG GCTGGTGGAG
GCCGACGTGG AGGCTCACCC CGTGCTGGCT CTGACCCGGG AGTGGGAGGC
CCTGGAGGAC GAGGAGCGCG CGAAGAGCGC CCGGGCGATG GAGGTGTACG
CGGCGATGGT GGAGCGCATG GATTGGAACA TTGGCCGGGT GGTCGACTAC
CTGCGCCGGC AGGGCGAGCT GGACAACACC TTCGTGCTGT TCATGAGCGA
CAACGGTGCT GAGGGTGCCC TGCTGGAGGC CTTCCCGAAG TTTGGGCCGG

ACCTGCTGGG CTTTCTGGAC CGGCACTACG ACAACTCCCT GGAGAACATT
GGCCGCGCTA ACAGCTACGT GTGGTACGGC CCCCGCTGGG CCCAGGCGGC
CACCGCCCCC TCGCGCCTGT ACAAGGCTTT CACGACCCAA GGCGGCATTC
GCGTCCCCGC GCTCGTGCGC TACCCGCGCC TGTCCCGCCA AGGGGCTATT
TCCCACGCTT TCGCGACCGT GATGGACGTG ACGCCGACTC TCCTCGACCT
CGCCGGGGTG CGGCACCCGG GTAAGCGGTG GCGCGGCCGC GAGATTGCCG
AGCCGCGCGG CCGCAGCTGG CTGGGCTGGC TGAGCGGCGA GACTGATGCT
GCCCACGACG AGAACACTGT GACCGGCTGG GAGCTGTTCG GCATGCGCGC
GATCCGCCAG GGCGACTGGA AGGCGGTGTA CCTGCCTGCC CCTGTGGGCC
CCGCGACCTG GCAGCTGTAC GACCTGGCGC GGGACCCGGG TGAGATCCAC
GACCTCGCTG ACTCCCAGCC CGGCAAGCTG GCTGAGCTGA TCGAGCATTG
GAAGCGCTAC GTGTCCGAGA CCGGCGTGGT GGAGGGCGCC AGCCCCTTCC
TGGTGCGG

Alcalase ATGCGGAGCA AGAAGCTGTG GATCTCCCTG CTGTTCGCCC TCACGCTGAT
CTTCACCATG GCGTTCTCCA ACATGAGCGC GCAGGCGGCC GGGAAGAGCA
GCACGGAGAA GAAGTACATC GTGGGCTTCA AGCAGACTAT GAGCGCCATG
TCGTCCGCGA AGAAGAAGGA CGTCATTTCG GAGAAGGGCG GGAAGGTCCA
GAAGCAGTTC AAGTACGTCA ACGCCGCCGC CGCTACGCTG GACGAGAAGG
CGGTCAAGGA GCTGAAGAAG GATCCCTCCG TCGCGTACGT GGAGGAGGAC
CATATTGCCC ATGAGTACGC TCAGTCGGTG CCTTACGGCA TCAGCCAGAT
CAAGGCGCCG GCCCTGCACA GCCAGGGTTA CACCGGCAGC AACGTCAAGG
TCGCTGTCAT CGACAGCGGC ATCGACAGCA GCCACCCCGA CCTGAACGTG
CGGGGCGGCG CCTCGTTCGT GCCCTCGGAG ACCAACCCCT ACCAGGATGG
CTCCAGCCAC GGCACCCACG TGGCGGGGAC GATCGCCGCG CTGAACAACT
CGATTGGCGT CCTGGGCGTG GCGCCCTCCG CTAGCCTGTA CGCCGTGAAG
GTGCTGGACA GCACCGGCAG CGGCCAGTAC TCCTGGATCA TCAACGGCAT
CGAGTGGGCG ATCAGCAACA ACATGGACGT GATCAACATG AGCCTGGGCG
GCCCGACGGG CTCCACTGCC CTGAAGACTG TGGTCGACAA GGCTGTGTCC
AGCGGCATCG TGGTGGCCGC GGCGGCTGGC AACGAGGGCT CCTCCGGCAG
CACGTCCACG GTGGGGTACC CCGCCAAGTA CCCTTCCACT ATCGCGGTGG
GCGCCGTCAA CTCGAGCAAC CAGCGCGCCT CCTTCAGCTC GGCCGGCTCG
GAGCTGGACG TGATGGCTCC GGGCGTGAGC ATCCAGTCCA CTCTGCCCGG
CGGCACCTAC GGCGCCTACA ACGGCACCAG CATGGCGACG CCTCATGTGG
CGGGGGCGGC CGCCCTCATC CTGAGCAAGC ACCCCACGTG GACCAACGCC
CAGGTCCGCG ACCGGCTGGA GTCCACCGCC ACGTACCTCG GCAACTCCTT
CTACTATGGC AAGGGCCTGA TCAACGTGCA AGCCGCTGCG CAG

Lysozyme ATGAACGCGA AGATCCGCTA CGGCCTGTCC GCCGCCGTGC
TCGCCCTGAT CGGGGCGGGC GCGAGCGCCC CCGAGATCCT GGATCAGTTC
CTGGACGAGA AGGAGGGCAA CCACACCACC GCTTACCGCG ACGGCGCCGG
CATCTGGACG ATTTGCCGCG GCGCCACGCG CGTGGACGGC AAGCCCGTGA
TCCCGGGCAT GAAGCTGTCG AAGGAGAAGT GCGACCGCGT GAACGCCATT
GAGCGCGACA AGGCCCTGGC CTGGGTGGAG AAGAACATCC GCGTGCCCCT
GACCGAGCCG CAGAAGGCCG GTATCGCGAG CTTCTGCCCC TACAACATTG
GCCCCGGCAA GTGCTTTCCG AGCACCTTCT ACCGCCGCAT CAACGCCGGC

GACCGGAAGG GCGCCTGCGA GGCGATCCGG TGGTGGATCA AGGACGGCGG
CCGCGACTGC CGCATTCGCT CCAACAACTG CTACGGCCAA GTGTCGCGGC
GCGATCAGGA GTCGGCCCTG GCCTGCTGGG GGATCGACCG C

For just lysozyme:
LDSP
forward AAGATGGAGTGGATGGAGGAGG
reverse TATCGGATCTTCGCGTTCAT ATCTTATTGCCCCCCGG
lysozyme
forward ATGAACGCGAAGATCCGATACG
reverse ACTGGTGATTTTTGCGGACT tta tcgGTCgATTCCCCAGCAGG

For just sulfatase:
LDSP
forward AAGATGGAGTGGATGGAGGAGG
reverse AAGTTaGGtCGCTTGGACAT ATCTTATTGCCCCCCGG
sulfatase
forward ATGTCCAAGCGaCCtAACTTCC
reverse ACTGGTGATTTTTGCGGACT tta GCGaACCAGGAAGGGGGA

For just alcalase:
LDSP
forward AAGATGGAGTGGATGGAGGAGG
reverse CAGAGCTTCTTGGAGCGCAT ATCTTATTGCCCCCCGG
alcalase
forward ATGCGCTCCAAGAAGCTCTGGA
reverseACTGGTGATTTTTGCGGACTttaCTGaGCaGCGGCCTGGACGTTGAT

For all three on one:
LDSP
forward AAGATGGAGTGGATGGAGGAGG
reverse AAGTTaGGtCGCTTGGACAT ATCTTATTGCCCCCCGG
sulfatase
forward CCGGGGGGCAATAAGAT ATGTCCAAGCGaCCtAACTTCC
reverseCAGAGCTTCTTGGAGCGCATCCCCTGGAAGTAAAGGTTCTC
GCGaACCAGGAAGGGGGA
alcalase
forward GAGAACCTTTACTTCCAGGGG ATGCGCTCCAAGAAGCTCTGGA
reverseTATCGGATCTTCGCGTTCATCCCCTGGAAGTAAAGGTTCTC
CTGaGCaGCGGCCTGGACGTTGAT
lysozyme
forward GAGAACCTTTACTTCCAGGGG ATGAACGCGAAGATCCGATACG
reverse ACTGGTGATTTTTGCGGACT TTA tcgGTCgATTCCCCAGCAGG
35S
forward GCTGGGGAATCGACcgaTAA AGTCCGCAAAAATCACCAGT
reverse GTCACTGGATTTTGGTTTTAGG

The sequences were assembled into an IDTvector with a xeocin selection marker. This was achieved using PCR assembly using 20-30 PCR cycles per addition and a commercial stabilized T5 exonuclease. The largest plasmid, containing all three heterologous genes, selection marker, and promoter/terminator sequences was confirmed to be ~9.6kB by gel chromatography. The resulting plasmids were introduced into axenic *N. salina* cells using the electroporation protocol established by Kilian et al. (Kilian et al., 2011). Zeocin-resistant colonies obtained by transformation were resuspended in 50 µL F/2 medium lacking any nitrogen source, and 6 µL was spotted on agar plates containing 1 mM KNO_3. After ~2 days the cells were observed to bleach indicating depletion of the nitrogen source and expression of the homologous enzymes. The peptide antibody against each of the deconstruction enzyes was produced by Covance Nonclinical Services using the C-terminal peptide [H]-CVPALDKVLANKKVAKFLLK-[NH2]. For immunoblot analysis, cell pellets were extracted with sample buffer to yield 50,000 cells/μL. Extracts were diluted 10-, 20-, and 50-fold, and 20 μL was loaded onto a 15% SDS-PAGE gel. Gel electrophoresis and electroblotting was performed with a Bio-Rad Mini Protean system according to the manufacturer's instructions (Bio-Rad Life Sciences). Anti-sulfatase, alcalase, and lysozme antibodies was used in a 1:10,000 dilution. Quantification was performed densitometrically using ImageJ software (National Institutes of Health) on immunoblots with immunoreactive proteins visualized using alkaline phosphatase. The results indicated successful expression of each of the proteins.

6. REFERENCES

AZACHI, M., SADKA, A., FISHER, M., GOLDSHLAG, P., GOKHMAN, I., ZAMIR, A. 2002. SALT INDUCTION OF FATTY ACID ELONGASE AND MEMBRANE LIPID MODIFICATIONS IN THE EXTREME HALOTOLERANT ALGA *DUNALIELLA SALINA. PLANT PHYSIOL*, 129(3), 1320-9.

BEN-AMOTZ, A., AVRON, M. 1982. THE POTENTIAL USE OF *DUNALIELLA* FOR THE PRODUCTION OF GLYCEROL, B-CAROTENE, AND HIGH-PROTEIN FEED. IN: *BIOSALINE RESEARCH: A LOOK TO THE FUTURE*, (ED.) A. SAN PIETO, PLENUM PUB. CORP. NEW YORK, PP. 207-214.

BOROWITZKA, M.A. 1986. MICROALGAE AS SOURCES OF FINE CHEMICALS. *MICROBIOL SCI*, 3(12), 372-375.

CHAPMAN, K.D., OHLROGGE, J.B. 2012. COMPARTMENTATION OF TRIACYLGLYCEROL ACCUMULATION IN PLANTS. *J BIOL CHEM*, 287(4), 2288-94.

DAHLQVIST, A., STAHL, U., LENMAN, M., BANAS, A., LEE, M., SANDAGER, L., RONNE, H., STYMNE, H. 2000. PHOSPHOLIPID : DIACYLGLYCEROL ACYLTRANSFERASE: AN ENZYME THAT CATALYZES THE ACYL-COA-INDEPENDENT FORMATION OF TRIACYLGLYCEROL IN YEAST AND PLANTS. *PROC NATL ACAD SCI U S A*, 97(12), 6487-6492.

DAVIS, R.W., CARVALHO, B.J., JONES, H.D.T., SINGH, S. 2014A. THE ROLE OF PHOTO-OSMOTIC ADAPTATION IN SEMI-CONTINUOUS CULTURE AND LIPID RELEASE FROM *DUNALIELLA VIRIDIS*. *JOURNAL OF APPLIED PHYCOLOGY*.

DAVIS, R.W., JONES, H.D.T., COLLINS, A.M., RICKEN, J.B., SINCLAIR, M.B., TIMLIN, J.A., SINGH, S. 2013. LABEL-FREE MEASURMENT OF ALGAL TRIACYLGLYCERIDE PRODUCTION USING FLUORESCENCE HYPERSPECTRAL IMAGING. *ALGAL RESEARCH*.

DAVIS, R.W., WU, W., SINGH, S. 2014B. MULTISPECTRAL SORTER FOR RAPID, NONDESTRUCTIVE OPTICAL BIOPROSPECTING FOR ALGAE BIOFUELS. *PROC SPIE*, 8947.

DE OLIVEIRA, V.E., CASTRO, H.V., EDWARDS, H.G.M., DE OLIVEIRA, L.F.C. 2010. CAROTENES AND CAROTENOIDS IN NATURAL BIOLOGICAL SAMPLES: A RAMAN SPECTROSCOPIC ANALYSIS. *JOURNAL OF RAMAN SPECTROSCOPY*, 41(6), 642-650.

GELIN, F., BOOGERS, I., NOORDELOOS, A.A.M., RIEGMAN, R., DE LEEUW, J.W. 1997. RESISTANT BIOMACROMOLECULES IN MARINE MICROALGAE OF THE CLASSES EUSTIGMATOPHYCEAE AND CHLOROPHYCEAE: GEOCHEMICAL IMPLICATIONS. *ORGANIC GEOCHEMISTRY*, 26, 413-424.

GOODSON, C., ROTH, R., WANG, Z.T., GOODENOUGH, U. 2011. STRUCTURAL CORRELATES OF CYTOPLASMIC AND CHLOROPLAST LIPID BODY SYNTHESIS IN CHLAMYDOMONAS REINHARDTII AND STIMULATION OF LIPID BODY PRODUCTION WITH ACETATE BOOST. *EUKARYOTIC CELL*, 10(12), 1592-1606.

GREENWELL, H.C., LAURENS, L.M., SHIELDS, R.J., LOVITT, R.W., FLYNN, K.J. 2010. PLACING MICROALGAE ON THE BIOFUELS PRIORITY LIST: A

REVIEW OF THE TECHNOLOGICAL CHALLENGES. *J ROY SOC INTERF*, 7(46), 703-26.

HANSON, M.R., SATTARZADEH, A. 2011. STROMULES: RECENT INSIGHTS INTO A LONG NEGLECTED FEATURE OF PLASTID MORPHOLOGY AND FUNCTION. *PLANT PHYSIOL*, 155(4), 1486-1492.

JIAO, G., YU, G., ZHANG, J., EWART, H.S. 2011. CHEMICAL STRUCTURES AND BIOACTIVES OF SULFATED POLYSACCHARIDES FROM MARINE ALGAE. *MARINE DRUGS*, 9(196-223).

KILIAN, O., BENEMANN, C.S., NIYOGI, K.K., VICK, B. 2011. HIGH-EFFICIENCY HOMOLOGOUS RECOMBINATION IN THE OIL-PRODUCING ALGA NANNOCHLOROPSIS SP. *PROC NATL ACAD SCI U S A*, 108(52), 21265-9.

KLEINEGRIS, D., VAN ES, M., JANSSEN, M., BRANDENBURG, W., WIJFFELS, R. 2010. CAROTENOID FLUORESCENCE IN *DUNALIELLA SALINA*. *JOURNAL OF APPLIED PHYCOLOGY*, 22(5), 645-649.

KOHLER, R.H., CAO, J., ZIPFEL, W.R., WEBB, W.W., HANSON, M.R. 1997. EXCHANGE OF PROTEIN MOLECULES THROUGH CONNECTIONS BETWEEN HIGHER PLANT PLASTIDS. *SCIENCE*, 276(5321), 2039-2042.

KRAMER, D.M., JOHNSON, G., KIIRATS, O., EDWARDS, G.E. 2004. NEW FLUORESCENCE PARAMETERS FOR THE DETERMINATION OF *QA* REDOX STATE AND EXCITATION ENERGY FLUXES. *PHOTOSYNTH RES*, 79, 209-218.

LEMOINE, Y., SCHOEFS, B. 2010. SECONDARY KETOCAROTENOID ASTAXANTHIN BIOSYNTHESIS IN ALGAE: A MULTIFUNCTIONAL RESPONSE TO STRESS. *PHOTOSYNTHESIS RESEARCH*, 106(1), 155-177.

LISKA, A.J., SHEVCHENKO, A., PICK, U., KATZ, A. 2004. ENHANCED PHOTOSYNTHESIS AND REDOX ENERGY PRODUCTION CONTRIBUTE TO SALINITY TOLERANCE IN *DUNALIELLA* AS REVEALED BY HOMOLOGY-BASED PROTEOMICS. *PLANT PHYSIOL*, 136(1), 2806-17.

MERCER, P., ARMENTA, R.E. 2011. DEVELOPMENTS IN OIL EXTRACTION FORM MICROALGAE. *EUROPEAN JOURNAL OF LIPID SCIENCE AND TECHNOLOGY*, 113(5), 539-547.

MOLINA GRIMA, E., BELARBI, E.-H., ACIEN FERNANDEZ, F.G., ROBLES MEDINA, A., CHISTI, Y. 2003. RECOVERY OF MICROALGAL BIOMASS AND METABOLITES: PROCESS OPTIONS AND ECONOMICS. *BIOTECHNOLOGY ADVANCES*, 20, 491-515.

MOULIN, P., LEMOINE, Y., SCHOEFS, B. 2010. MODIFICATIONS OF THE CAROTENOID METABOLISM IN PLASTIDS. IN: *HANDBOOK OF PLANT AND CROP STRESS, THIRD EDITION*, CRC PRESS, PP. 407-433.

MOULTON, T.P., BOROWITZKA, L.J., VINCENT, D.J. 1987. THE MASS-CULTURE OF *DUNALIELLA SALINA* FOR BETA-CAROTENE - FROM PILOT-PLANT TO PRODUCTION PLANT. *HYDROBIOLOGIA*, 151, 99-105.

NGUYEN, H.M., BAUDET, M., CUINE, S., ADRIANO, J.M., BARTHE, D., BILLON, E., BRULEY, C., BEISSON, F., PELTIER, G., FERRO, M., LI-BEISSON, Y. 2011. PROTEOMIC PROFILING OF OIL BODIES ISOLATED FROM THE UNICELLULAR GREEN MICROALGA CHLAMYDOMONAS REINHARDTII:

WITH FOCUS ON PROTEINS INVOLVED IN LIPID METABOLISM. *PROTEOMICS*, 11(21), 4266-73.

QUIRANTES, A., BERNARD, S. 2004. LIGHT SCATTERING BY MARINE ALGAE: TWO-LAYER SPHERICAL AND NONSPHERICAL MODELS. *JOURNAL OF QUANTITATIVE SPECTROSCOPY & RADIATIVE TRANSFER*, 89(1-4), 311-321.

ROBERT, B. 1999A. THE ELECTRONIC STRUCTURE, STEREOCHEMISTRY AND RESONANCE RAMAN SPECTROSCOPY OF CAROTENOIDS. IN: *THE PHOTOCHEMISTRY OF CAROTENOIDS*, (EDS.) H. FRANK, A. YOUNG, G. BRITTON, R. COGDELL, VOL. 8, SPRINGER NETHERLANDS, PP. 189-201.

ROBERT, B. 1999B. THE ELECTRONIC STRUCTURE, STEREOCHEMISTRY AND RESONANCE RAMAN SPECTROSCOPY OF CAROTENOIDS. . IN: *PHOTOCHEMISTRY OF CAROTENOIDS*, (EDS.) H. FRANK, A. YOUNG, G. BRITTON, R. COGDELL, VOL. 8, SPRINGER. NETHERLANDS, PP. 189-201.

RODOLFI, L., ZITTELLI, G.C., BASSI, N., PADOVANI, G., BIONDI, N., BONINI, G., TREDICI, M.R. 2009. MICROALGAE FOR OIL: STRAIN SELECTION, INDUCTION OF LIPID SYNTHESIS AND OUTDOOR MASS CULTIVATION IN A LOW-COST PHOTOBIOREACTOR. *BIOTECHNOLOGY AND BIOENGINEERING*, 102(1), 100-112.

SCHREIBER, U. 2004. PULSE-AMPLITUDE (PAM) FLUOROMETRY AND SATURATION PULSE METHOD. IN: *CHLOROPHYLL FLUORESCENCE: A SIGNATURE OF PHOTOSYNTHESIS*, (EDS.) G. PAPAGEORGIOU, GOVINDJEE, KLUWER ACADEMIC PUBLISHERS. DORDECHT, THE NETHERLANDS, PP. 279-319.

TAN, C., QIN, S., ZHANG, Q., JIANG, P., ZHAO, F. 2005. ESTABLISHMENT OF A MICRO-PARTICLE BOMBARDMENT TRANSFORMATION SYSTEM FOR *DUNALIELLA SALINA*. *JOURNAL OF MICROBIOLOGY*, 43(4), 361-5.

TAYLOR, L.E.I., DAI, Z., DECKER, S.R., BRUNECKY, R., ADNEY, W.S., DING, S.-Y., HIMMEL, M.E. 2008. HETEROLOGOUS EXPRESSION OF GLYCOSYL HYDROLASES IN *PLANTA*: A NEW DEPARTURE FOR BIOFUELS. *TRENDS IN BIOTECHNNOLOGY*, 26(8), 413-424.

TORNABENE, T.G., HOLZER, G., PETERSON, S.L. 1980. LIPID PROFILE OF THE HALOPHILIC ALGA, *DUNALIELLA SALINA. BIOCHEMICAL AND BIOPHYSICAL RESEARCH COMMUNICATIONS*, 96(3), 1349-1356.

VIELER, A., BRUBACKER, S.B., VICK, B., BENNING, C. 2012. A LIPID DROPLET PROTEIN OF *NANNOCHLOROPSIS* WITH FUNCTIONS PARTIALLY ANALOGOUS TO PLANT OLEOSINS. *PLANT PHYSIOLOGY* 158(4), 1562-9.

WEI, L., XIN, Y., WANG, D., JING, X., ZHOU, Q., SU, X., JIA, J., NING, K., CHEN, F., HU, Q., XU, J. 2013. *NANNOCHLOROPSIS* PLASTID AND MITOCHONDRIAL PHYLOGENOMES REVEAL ORGANELLE DIVERSIFICATION MECHANISM AND INTRAGENUS PHYLOTYPING STRATEGY IN MICROALGAE. *BMC GENOMICS*, 14.

WIJFFELS, R.H., BARBOSA, M.J., EPPINK, M.H.K. 2010. MICROALGAE FOR THE PRODUCTION OF BULK CHEMICALS AND BIOFUELS. *BIOFUELS BIOPROD BIOREFIN*, 4, 287-295.

WU, H., VOLPONI, J.V., OLIVER, A.E., PARIKH, A.N., SIMMONS, B.A., SINGH, S. 2011. *IN VIVO* LIPIDOMICS USING SINGLE-CELL RAMAN SPECTROSCOPY. *P NATL ACAD SCI USA*, 108(9), 3809-14.

YOON, K., HAN, D.X., LI, Y.T., SOMMERFELD, M., HU, Q. 2012. PHOSPHOLIPID:DIACYLGLYCEROL ACYLTRANSFERASE IS A MULTIFUNCTIONAL ENZYME INVOLVED IN MEMBRANE LIPID TURNOVER AND DEGRADATION WHILE SYNTHESIZING TRIACYLGLYCEROL IN THE UNICELLULAR GREEN MICROALGA CHLAMYDOMONAS REINHARDTII. *PLANT CELL*, 24(9), 3708-3724.

DISTRIBUTION

1	MS0359	D. Chavez, LDRD Office	1911


Sandia National Laboratories